Published in final edited form as:
J Mol Biol. 2010 July 16; 400(3): 354–378. doi:10.1016/j.jmb.2010.04.065.

The Macroscopic Rate of Nucleic Acid Translocation by Hepatitis C virus Helicase NS3h is Dependent on Both the Sugar and Base Moieties

Ali R. Khaki[1], **Cassandra Field**[2], **Shuja Malik**[2], **Anita Niedziela-Majka**[1], **Stephanie A. Leavitt**[1], **Ruth Wang**[1], **Magdeleine Hung**[1], **Roman Sakowicz**[1], **Katherine M. Brendza**[1], and **Christopher J. Fischer**[2,*]

[1] Gilead Sciences, Inc., 333 Lakeside Dr., Foster City, CA 94404

[2] University of Kansas Department of Physics and Astronomy, 1082 Malott Hall, 1251 Wescoe Hall Dr., Lawrence, KS 66045

Abstract

The NS3 helicase (NS3h) of hepatitis C virus (HCV) is a 3′ to 5′ SF2 RNA and DNA helicase that is essential for the replication of HCV. We have examined the kinetic mechanism of translocation of NS3h along single-stranded nucleic acid with bases rU, dU and dT and have found that the macroscopic rate of translocation is dependent upon both the base and sugar moieties of the nucleic acid, with approximate macroscopic translocation rates of 3 nt/s (oligo-dT), 35 nt/s (oligo-dU), and 42 nt/s (oligo-rU), respectively. We found a strong correlation between the macroscopic translocation rates and the binding affinity of the translocating NS3h protein to the respective substrates such that weaker affinity corresponded to faster translocation. The values of $K_{0.5}$ for NS3h translocation at a saturating ATP concentration are: (3.3 ± 0.4) μM nucleotide (poly-dT), (27 ± 2) μM nucleotide (poly-dU), and (36 ± 2) μM nucleotide (poly-rU). Furthermore, the results of isothermal titration of NS3h with these oligonucleotides suggest that differences in TΔS° are the principal source of the differences in the affinity of NS3h binding to these substrates. Interestingly, despite the differences in macroscopic translocation rates and binding affinities, the ATP coupling stoichiometry for NS3h translocation was identical for all three substrates, ~0.5 ATP molecules consumed per nucleotide translocated. This similar periodicity of ATP consumption implies a similar mechanism for NS3h translocation along RNA and DNA substrates.

Keywords

NS3 helicase; translocation; nucleic acid; ATPase; mechanism

INTRODUCTION

Helicases are motor proteins that utilize the energy generated through ATP binding and hydrolysis for translocation along single-stranded nucleic acids and unwinding of double-

*To whom the correspondences should be addressed: Christopher J. Fischer, University of Kansas, Department of Physics and Astronomy, 1082 Malott Hall, 1251 Wescoe Hall Drive, Lawrence, KS, 66045. Phone: 785-864-4579, Fax: 785-864-5262, shark@ku.edu.

stranded nucleic acids.[1; 2; 3; 4; 5] Members of this ubiquitous class of proteins play a vital role in DNA and RNA metabolism participating in many critical processes including replication, recombination, and repair.[6; 7] Hepatitis C virus (HCV) is a single-stranded RNA virus that requires several virally encoded proteins for successful replication. One of the proteins that is essential for viral replication is non-structural protein 3 (NS3).[8] NS3 is a multifunctional protein that possesses N-terminal protease activity and C-terminal NTPase and helicase activity.[9; 10] Both protease and helicase activities are required for viral replication.[11] The helicase domain of NS3 is a member of helicase superfamily 2 (SF2)[12] and is capable of unwinding both RNA and DNA[13] duplexes with a 3′ to 5′ directional bias[9; 12; 13] and translocating along single-stranded DNA with an identical 3′ to 5′ directional bias.[14]

Based upon the initial structural study performed on the helicase domain of NS3 (NS3h), it was suggested that previously observed differences in the affinity of NS3h binding to a series of short oligonucleotides and the corresponding differences in the stimulation of the ATPase activity of NS3h in the presence of these same oligonucleotides were to a large extent dominated by differences in the entropic contributions to the free energies of NS3h binding to these substrates.[15] Furthermore, based upon the observation that the oligonucleotide bound to NS3h in their crystal structure was slightly bent, these same authors suggested that these differences in the entropic contribution to the free energies of binding are associated with the deformation of the substrates themselves.[15] More recent crystal structures of NS3h bound to oligo-dU showed that the contacts between NS3h and the nucleic acid were largely limited to the phosphate backbone. [16] These studies revealed three distinct crystals of NS3h together with single-stranded DNA and different ATP analogs, leading to the proposal of a physical model for DNA translocation by NS3h where changes in the intradomain structure of the enzyme were directly coupled to the structural transitions of the associated DNA. [16] Based upon this model, these authors further speculated that the preference of the ribose sugar to adopt a C3′-endo sugar pucker rather than a C2′-endo sugar pucker would favor NS3h binding to DNA over RNA. Subsequently, based on their results, one would expect that these differences in NS3h binding would translate into variability in translocation behavior along DNA and RNA.

Recent biochemical studies on NS3 catalyzed nucleic acid unwinding have been used to explain nucleic acid translocation by NS3, [17; 18; 19; 20; 21] though a clear mechanism of action for either of these processes has not been identified. Two primary models have been used to describe the mechanism of unwinding and translocation by NS3. The first is a Brownian motor mechanism for unwinding and translocation, which is based on NS3h substrate binding studies in the presence and absence of ATP.[18; 19] The second is the more commonly accepted inchworm model, initially suggested in lieu of structural evidence.[15] Recent biochemical studies with full-length NS3 using single-molecule fluorescence resonance energy transfer (FRET) and optical tweezers have also supported this model.[17; 20; 21] Furthermore, a similar model has been suggested for the SF1 helicase PcrA.[22; 23; 24] Experiments performed for NS3 assuming the inchworm model have identified large and small step sizes of 11–18 base pairs (bp) [17; 21] and 3 bp, [17; 20] respectively. The small step size was further shown to consist of three 1 bp “hidden steps.” Therefore, each 1 bp step was shown to correspond to the hydrolysis of one ATP.[20] A large physical step size for single-stranded nucleic acid translocation is also suggested by the fact that NS3 has been shown to tolerate large disruptions in its nucleic acid tracking strand during double-stranded nucleic acid unwinding.[25]

In order to better understand the mechanism of action of this helicase, we performed a series of pre-steady-state stopped-flow experiments to determine the macroscopic translocation rates along 5′ fluorescently labeled, single-stranded oligonucleotides. In this study, we

utilized various lengths of oligodeoxythymidylate (dT), oligodeoxyuridylate (dU), and oligouridylate (rU) to measure the macroscopic translocation rates and coordinated these rates with ATP consumption based on ATPase stimulation experiments using poly-dT, poly-dU, and poly-rU substrates. Lastly, we independently determined the K_d for NS3h binding to poly-dT and poly-dU to further complement the translocation experiments. The work presented here is first reported rigorous analysis of the dependence of nucleic acid translocation of NS3h on the base and sugar moieties of the nucleic acid.

RESULTS

Our first step in characterizing the kinetics of nucleic acid translocation by NS3h was to confirm that the solution conditions to be used would be appropriate for monitoring the translocation activity of the enzyme. The results of sedimentation velocity experiments demonstrated that NS3h is monomeric under the solution conditions of 25 mM MOPS (pH 7.0), 30 mM NaCl, 5 mM $MgCl_2$, 2 mM DTT, 1% glycerol, and 25 °C (Figure 1); these conditions are subsequently referred to as translocation buffer (see Materials and Methods). As shown in Figure 1A, the c(s) distribution calculated for 15, 7.5, 3.75 and 1.87 μM NS3h spun in translocation buffer at 25°C displayed a single, symmetrically shaped peak, and the peak position did not change with protein concentration. These data are consistent with the presence of a single oligomeric NS3h species in solution under these conditions. From the peak of c(s) distribution, the $s_{20,w}$ was calculated to be (3.64 ± 0.03) S (an average and standard deviation calculated at four different protein concentrations). The sample weight average $s_{20,w}$ value is also invariant over the range of NS3h concentrations examined (Figure 1B) and, furthermore, is comparable to the $s_{20,w}$ value calculated from the peak of c(s) distribution, thus indicating that the NS3h sample is homogeneous. The molecular weight of the species can be estimated by converting the c(s) distribution into c(M) distribution. The peak of c(M) distribution occurs at (45.9 ± 0.8) kDa, which is slightly smaller (~ 5.7%) than predicted from protein amino acid sequence monomer molecular weight of 48.6 kDa, but still consistent with NS3h existing as a monomer under these solution conditions. Finally, the value of the frictional coefficient ratio estimated from our results (f/f_0 = 1.17 ± 0.01) suggests that NS3h has a globular hydrodynamic shape (see Materials and Methods).

Additional sedimentation velocity experiments were then performed to determine the stoichiometry of complexes of NS3h with a short oligo-dT (dT_8) labeled on the 3′ end with a Cy5 fluorophore (5′-dT_8-Cy5-3′). In these experiments the absorbance of the Cy5 fluorophore at 648 nm was monitored in order to observe the sedimentation of the DNA without interference from the absorbance of NS3h. These experiments were performed at different ratios of the NS3h monomer to DNA in translocation buffer at 25°C. The data were analyzed using the c(s) approach (see Materials and Methods) and the resulting distributions (see Figure 2A) show two well resolved and symmetrical peaks centered at apparent sedimentation coefficients of (0.98 ± 0.03) S and (4.09 ± 0.06) S (these sedimentation coefficients are not corrected to the standard conditions). The position of the first peak coincides with the position measured for the single-stranded DNA alone (black line in Figure 2A) and thus represents the sedimentation coefficient of the free DNA. The peak centered at approximately 4.09 S is present only for samples containing both the NS3h monomer and the DNA and thus can be associated with the NS3h-DNA complex. The position of first peak in c(s) distribution did not change with increasing NS3h concentration indicating that it is associated with a distinct species (free DNA) present in solution. The peak associated with the NS3h-DNA complex shifts marginally to higher sedimentation coefficient values with increasing NS3h concentrations, suggesting that the formation of the complex occurs on a time scale comparable to the time scale of sedimentation velocity experiment.

The results of these experiments were further analyzed by plotting the weight average sedimentation coefficients as a function of the molar ratio of the NS3h monomer to DNA in order to construct a binding isotherm. Even though an estimate of the equilibrium binding constant cannot be determined from the analysis of this binding isotherm, we can nevertheless determine an estimate of the stoichiometry of the NS3h-DNA complex (see Figure 2B). The two straight lines to which binding isotherm was fitted intersect at [NS3h]/[DNA] ratio of 1.4, suggesting that a single monomer of NS3h binds to 5′-dT_8-Cy5-3′ under these solution conditions. This stoichiometry is also consistent with the reported crystal structures of NS3h in complex with a single eight nucleotide oligo-dU [15] and with a single six nucleotide oligo-dT and oligo-dA [16].

Finally, in order to examine the possibility that NS3h binds cooperatively to nucleic acid we performed an additional set of sedimentation velocity experiments using a 19 nt single-stranded DNA substrate. As shown in Figure 2C, as the concentration of NS3h used in these experiments increases, the peak in the c(s) profile corresponding to free DNA decreases and a new peak, corresponding to a NS3h:DNA complex increases. This peak representing the complex also shifts to higher sedimentation coefficients as the molar ratio of NS3h to DNA increases, indicating that multiple NS3h molecules are capable of binding to a single DNA substrate. However, at a molar ratio of [NS3h]:[DNA] ≤ 1, the position of the peak representing the complex changes only marginally and is characterized by a sedimentation coefficient value expected for a monomer of NS3h bound to the DNA substrate. Therefore, when the molar ratio of [NS3h]:[DNA] ≤ 1, monomeric complexes of NS3h and DNA are formed exclusively; the formation of complexes containing two and possibly three molecules of NS3h requires significantly higher concentrations of protein. This behavior suggests that binding is not cooperative.

Affinity of DNA binding by NS3h depends upon the presence of fluorophores

The binding of monomers of NS3h to short fluorescently-labeled oligonuceotides in the absence of ATP was monitored by the changes in the fluorescence anisotropy that occur upon NS3h binding (see Materials and Methods). As shown in Figure 3A, the titration of NS3h into a solution containing a six nucleotide long oligo-dT (dT_6) labeled at either the 5′ end or the 3′ end with fluorescein (5′-F-dT_6 or 5′-dT_6-F) resulted in an increase in the fluorescence anisotropy. The magnitude of the change in anisotropy is larger for NS3h binding to 5′-F-dT_6 than for NS3h binding to 5′-dT_6-F (see below). It is worth mentioning that we also observed changes in the total fluorescence intensity of the fluorophore resulting from the binding of NS3h to both the 5′ and 3′ labeled DNA (~33% fluorescence intensity decrease and ~ 15% fluorescence intensity increase, respectively). Although the changes in fluorescence intensities occurring upon formation of NS3h-DNA complexes are small and do not significantly affect the estimates of the binding affinities, we have employed the appropriate correction[51,52] which accounts for those changes when calculating the fraction of fluorescent oligonucleotide bound to NS3h from the anisotropy data (Equation (4)). The binding affinities shown in Table 1 and Table 2 were obtained using the correction for the changes in fluorescein intensities due to protein binding. Based upon the results of our sedimentation velocity experiments, we analyzed the data in Figure 3A using a 1:1 binding model, Equation (4) and (5), for the association of NS3h and the DNA. The best fit parameters obtained from the analysis of the data in Figure 3A using Equation (4) and (5) are summarized in Table 1 and the solid lines in Figure 3A are simulations using these best fit parameters and Equation (4) and (5). As shown in Table 1, the affinity for NS3h binding to 5′-F-dT_6 was approximately eight times higher than the affinity for NS3h binding to 5′-dT_6-F, suggesting that the position of the fluorophore on the DNA affects the affinity of NS3h binding.

The differences in the magnitude of the change in the anisotropy of fluorescein fluorescence when the fluorophore is on either end of the DNA also suggest that NS3h binds to the DNA with a specific orientation or polarity. The anisotropy of the fluorophore-labeled DNA depends on both the rotational diffusion of the DNA and on the segmental motion of the fluorophore on the DNA. Therefore, the different changes in anisotropy observed in NS3h:DNA complexes when the fluorophore is on either end of the DNA may suggest that the rotational motion of the fluorophore on the DNA is different in the two cases. This possibility is, in fact, supported by our observation that the intensity of fluorescence emission is quenched upon the binding of NS3h to the dT_6 oligonucleotide (by ~ 33%) with fluorescein attached at its 5′ end in the absence of ATP whereas the fluorescence intensity increases as a result of complex formation on 3′ labeled dT_6 in the absence of ATP (by ~ 15%, data not shown). Hence, the environment in which the fluorescein fluorophore resides when in complex with NS3h is different when the fluorophore is on the 5′ or 3′ ends of the DNA. Moreover, the 5′ labeled dT_6 binds stronger to NS3h then the 3′ labeled oligonucleotide. Taken together, all of these data suggest that fluorescein at the 5′ end may interact with NS3h differently from how fluorescein at the 3′ end interacts in complex with the protein. Indeed, our results suggest that a fluorophore at the 5′ end may have restricted mobility when in complex with NS3h, resulting in higher anisotropy of the that complex in comparison to a complex between NS3h and DNA containing the fluorescein at the 3′ end, in which the fluorophore may be able to rotate more freely and thus have lower average anisotropy. Taken together, these data thus suggest that NS3h binds with a specific orientation or polarity with regard to the DNA and thus may lend insight into the mechanism by which directionally biased DNA translocation by NS3h (see below).

We monitored the binding of NS3h to an unlabeled dT_6 in the presence of 5′-F-dT_6 or 5′-dT_6-F in the absence of ATP using a competitive displacement assay (see Materials and Methods). In these experiments, shown in Figure 3B, a solution containing NS3h and either 5′-F-dT_6 or 5′-dT_6-F was titrated with dT_6 resulting in a decrease in the anisotropy as expected. The data in Figure 3B were analyzed using Equation (4) and (5) (see competition binding assay section in Materials and Methods). The best fit parameters obtained in this analysis are summarized in Table 1 and the solid lines in Figure 3B are simulations using Equation (4) and (5) and these best fit parameters. As demonstrated by the data in Table 1, the affinity of NS3h binding to 5′-F-dT_6 is approximately 12 times higher than the affinity for NS3h binding to dT_6, thus demonstrating that the presence of the fluorophore strongly affects the affinity of NS3h binding to the oligonucleotide.

Affinity of DNA binding by NS3h depends upon the nucleic acid base and sugar moieties

We next monitored the binding of NS3h to the non-fluorophore-labeled eight nucleotide nucleic acids dT_8, dU_8 and rU_8 using the same competition assay (see Materials and Methods). In these experiments, shown in Figure 4, a solution containing NS3h and either 5′-F-dT_6 (Figure 4A) or 5′-dT_6-F (Figure 4B) was titrated with dT_8, dU_8, or rU_8 and the resulting decrease in the anisotropy of the fluorescein labeled DNA reflected the shift in the NS3h binding equilibrium from 5′-F-dT_6 or 5′-dT_6-F to the unlabeled nucleic acids. The data in Figure 4 were analyzed using Equation (5) (see Materials and Methods). The best fit parameters obtained in this analysis are summarized in Table 2 and the solid lines in Figure 4 are simulations using Equation (5) and these best fit parameters. As demonstrated by the data in Table 2, NS3h binds with highest affinity to dT_8 and with lowest affinity to rU_8; the affinity for dU_8 is closer to that of rU_8 than to dT_8. These results indicate that the affinity of nucleic acid binding by NS3h is dependent upon both the sugar and base moieties.

NS3h is an ATP-dependent 3′ to 5′ nucleic acid translocase

Previous studies of the ATP-dependent single-stranded DNA translocation activity of the *B. stearothermophilus* PcrA monomer[26] and the *E. coli* UvrD monomer[27] have demonstrated that the net directionality of protein translocation can be determined by comparing the time courses of fluorescence observed from experiments in which a fluorophore is attached to the 3′ end of the DNA to those obtained from experiments in which the fluorophore is attached to the 5′ end of the DNA. Specifically, if translocation is biased toward the fluorophore, then the time courses of fluorescence will be characteristically dependent upon the length of the DNA, whereas if translocation is biased away from the fluorophore, then the time courses of fluorescence will be independent of the length of the DNA.[27] The fluorescence time courses shown in Figure 5 are associated with the translocation of NS3h along single-stranded oligo-dTs labeled at either the 3′ or 5′ end obtained from experiments conducted in translocation buffer at 25 °C under single-round conditions (single-round conditions were made possible by performing these experiments at a final heparin concentration of 4 mg/ml) as described in Materials and Methods. As shown in Figure 5, the time courses of fluorescence observed in these experiments are multi-phasic, regardless of the position of the fluorophore.

However, only the time courses obtained in experiments in which the fluorophore is on the 5′ end of the DNA display any dependence upon the length of the DNA (Figure 5A). As shown in Figure 5B, when the fluorescein fluorophore is attached to the 3′ end of the DNA, the qualitative shape of the observed time courses of fluorescence are independent of the length of the DNA. Taken together, these results indicate a 3′ to 5′ directionality to the translocation of NS3h along DNA.[28] It is not possible based upon the analysis of these data alone to interpret the mechanism by which the fluorescence intensity of the fluorophore changes upon the interaction of the fluorophore with the translocating NS3h monomer. However, some differences observed between the changes in fluorescence intensity observed in isothermal titrations of fluorescein labeled DNA with NS3h in the absence of ATP and the changes in fluorescence measured in translocation studies conducted in the presence of ATP do suggest that an ATP-dependent process is contributing to some of the observed differences in fluorescence. As elaborated more fully in the next section, this may be either a translocation initiation process or a multistep dissociation process. Nevertheless, this observation that NS3h binds to DNA with a preferred orientation is consistent with previously published results demonstrating that NS3 unwinds double-stranded nucleic acids with a 3′ to 5′ directional bias [9; 12; 13] and thus also with the model in which NS3 translocates along one strand of the double-stranded nucleic acid during unwinding.[25]

Moreover, the results of additional control experiments indicate that the time-dependent accumulation of NS3h at the 5′ end of the DNA substrates was not observed in the absence of ATP or in the presence of AMP-PNP, a slowly-hydrolysable ATP analogue (data not shown). Thus, both the binding and hydrolysis of ATP are required for NS3h translocation along DNA. Finally, the results of repeated experiments monitoring the oligonucleotide translocation of NS3h using this fluorescence based assay confirm that a final solution concentration of 1 mM ATP is saturating for NS3h translocation (data not shown).

Kinetic models for NS3h translocation

The simplest kinetic models consistent with the time courses in Figure 5 are shown in Scheme 1 and Scheme 2. In both of these models we assume that an NS3h monomer with a contact size of *d* nucleotides binds randomly, but uniformly and with polarity, to the single-stranded nucleic acid. We ignore any potential variations in the binding affinity of NS3h near the ends of the nucleic acid associated with differences in the counter-ion condensation at the ends.[29; 30] The NS3h monomer is initially bound *i* translocation steps away from the 5′ end with the value of *i* constrained ($1 \leq i \leq n$), where *n* is the number of translocation

steps needed for a NS3h monomer bound initially at the 3′ end of the single-stranded nucleic acid to move to the 5′ end.[27; 28; 31]

In Scheme 1, the NS3h monomer is initially bound in a translocation competent state (T_i state) and following the addition of ATP translocates from 3′ to 5′ along the single-stranded nucleic acid through a series of repeated rate-limiting translocation steps, with associated microscopic rate constant k_t. During each translocation step, the NS3h monomer moves m nucleotides and hydrolyzes c ATP molecules; the microscopic parameter m is referred to as the kinetic step size of translocation. The microscopic rate constant for dissociation during translocation is k_d and therefore the processivity of translocation is $P=\frac{k_t}{k_t+k_d}$. Upon reaching the 5′ end of the single-stranded nucleic acid, the NS3h monomer dissociates via a two step mechanism with successive rate constants k_c and k_{end}. Although our analysis of these kinetic time-courses indicates that NS3h dissociation from the 5′ end of the single-stranded nucleic acid occurs via a two-step process, the relative order of these two steps cannot be determined from our experiments. Upon dissociation from the single-stranded nucleic acid, the free NS3h protein is rapidly bound by the protein trap, heparin, and thus prevented from rebinding the single-stranded nucleic acid.

In Scheme 2, the NS3h monomer is initially bound in a conformation that is not competent for translocation (I_i state). Upon the addition of ATP, the NS3h monomer converts to a translocation competent conformation (the T_i state in Scheme 1) with an associated microscopic rate constant k_i. The NS3h monomer then translocates along the nucleic acid in a mechanism identical to that described for Scheme 1. Upon reaching the 5′ end of the nucleic acid, however, the NS3h monomer dissociates through a single step mechanism with an associated microscopic rate constant k_{end}. As with Scheme 1, any NS3h monomers that dissociate from the nucleic acid are bound by the protein trap and prevented from rebinding the nucleic acid.

For both Scheme 1 and Scheme 2, we define two macroscopic quantities of interest: the macroscopic translocation rate and the macroscopic ATP coupling stoichiometry. The macroscopic translocation rate, defined as the product $m*k_t$, has the units of nucleotides per second, and is a measure of the net rate of translocation from 3′ to 5′ along the single-stranded nucleic acid. Similarly, the macroscopic ATP coupling stoichiometry, defined as the ratio c/m, has the units of ATP hydrolyzed (or ADP produced) per nucleotide translocated and is a measure of the total ATP consumption (or ADP production) associated with the net forward motion (from 3′ to 5′) of the NS3h monomer along the single-stranded nucleic acid. Also, as described in Materials and Methods, the mathematical equations associated with both Scheme 1 and Scheme 2 incorporate directly the possibility of different affinities for NS3h binding to the 3′ end of the nucleic acid, to the 5′ end of the nucleic acid, and to all other positions on the nucleic acid.

Kinetic Characterization of Nucleic Acid Translocation by NS3h

Figure 6A shows a series of fluorescence time courses obtained in experiments conducted in translocation buffer at 25 °C under single-round conditions using a set of 5′ fluorescein labeled oligo-dTs with lengths of 53, 61, and 73 nt. As noted previously, single-round conditions were made possible by performing these experiments at a final heparin concentration of 4 mg/ml (see Materials and Methods). As described in Materials and Methods, these data were analyzed globally using Scheme 1 (Equation (7)); the solid lines in Figure 6A are simulations using Equation (7) and the best fit parameters obtained from this analysis. The average and standard deviation of the results obtained in the analysis of at least three independent sets of experimental time courses are shown in Table 3.

In the global NLLS analysis of the time courses in Figure 6A using Equation (7), the value of the parameter k_d (see Scheme 1) was one of the fitted variables (see Materials and Methods). This approach is different to that previously employed to characterize the kinetic mechanism of single-stranded DNA translocation by monomers of the *E. coli* UvrD helicase using similar stopped-flow fluorescence based experiments.[27; 31] In those studies, an independent estimate of the value of k_d was determined experimentally through the analysis of the time dependent change in the intrinsic tryptophan fluorescence of the UvrD monomers associated with the dissociation of UvrD monomers translocating along poly(dT).[27; 31] We performed a similar set of experiments with NS3h, but were unable to determine an estimate of k_d from the resulting data as changes in the intrinsic tryptophan fluorescence of NS3h associated with both the binding and the hydrolysis of ATP were of similar magnitude to the changes which were associated with the binding of poly(dT) or heparin (data not shown). A recent study of the DNA unwinding and translocation activity of NS3h and full-length NS3 reported similar changes in tryptophan fluorescence following DNA binding[14]. Due to this, we were unable to determine an independent estimate of k_d to use as a constraint in our NLLS analysis.

The principle reason that the authors of the previous study constrained the estimate of k_d in their analysis of the translocation time courses was to minimize the influence of parameter correlation on the estimates of the microscopic kinetic parameters in their model.[27; 28] Through repeatedly fitting our data with different constrained values of k_d, we have confirmed that both of our kinetic models also exhibit significant correlation among the microscopic parameters. However, we have also observed that despite this correlation, the estimates of the macroscopic translocation rate, the product of m and k_t, is always well constrained regardless of the individual estimates of the microscopic parameters in the model (data not shown). Furthermore, we have performed an additional series of computer simulations which confirmed that the estimate of the macroscopic translocation rate obtained from the NLLS analysis of translocation time courses acquired from these experiments using these models was always well constrained, even when non-uniform perturbations (backward motion, stalling, etc.) occur during the translocation of the enzyme along the nucleic acid (Fischer *et al.*, in preparation). Therefore, we are confident that our analysis allows for accurate estimation of the macroscopic translocation rate for NS3h along these oligonucleotides.

It is also worth noting that when the single-stranded DNA translocation activity of monomers of the *E. coli* UvrD helicase was characterized using similar stopped-flow fluorescence based experiments, the authors independently analyzed the results obtained from separate experiments using different fluorophores to obtain a fluorophore independent characterization of the translocation activity.[27] For this same reason, we also repeated our translocation experiments using oligo-dT labeled at the 5′ end with Cy3 (Figure 6B). As before, these data were analyzed globally using Scheme 1 (Equation (7)); the solid lines in Figure 6B are simulations using Equation (7) and the best fit parameters obtained from this analysis. The average and standard deviation of the results obtained in the analysis of at least three independent sets of experimental time courses are shown in Table 3. Interestingly, although several of the microscopic translocation parameters are fluorophore dependent, the estimate of the macroscopic translocation rate, (3.1 ± 0.3 nt/s) for fluorescein-labeled DNA and (2.7 ± 0.2 nt/s) for Cy3-labeled DNA, is independent of the fluorophore used. This is also consistent with the results of previously mentioned computer simulations that demonstrated that the estimate of the macroscopic translocation rate is well constrained by our analysis. A similar result was observed for the translocation of monomers of the *E. coli* UvrD helicase along single-stranded DNA.[27] In addition, the d and r parameters obtained from that analysis of the translocation time courses acquired in experiments performed with Cy3 labeled DNA are larger than the estimates of these parameters obtained from the

analysis of the translocation time courses acquired in experiments performed with fluorescein labeled DNA. A similar difference in the estimates of these parameters was obtained from the analysis of the time courses of UvrD translocation along fluorescein and Cy3 labeled DNA. This difference was hypothesized to result from an interaction distance between UvrD and Cy3 that was larger than that between UvrD and fluorescein.[27] A similar phenomenon may therefore explain the interaction between NS3h and these same fluorophores.

The quality of the global NLLS analysis of these same data sets according to Scheme 2 (Equation (9)), as judged by the standard deviation of the fits, was indistinguishable to that obtained with Scheme 1 (Equation (7)); the standard deviations for the NLLS analysis of the data with Equation (7) and Equation (9) were 9.4×10^{-4} and 9.5×10^{-4}, respectively. The estimates of the macroscopic translocation rates obtained with each model are also consistent with each other (Table 3 and Table 4). Thus we are unable to determine which kinetic mechanism is correct based upon these data alone.

Nucleic acid translocation by NS3h is dependent upon the nucleic acid base and sugar moieties

NS3h is unique in its ability to unwind both RNA and DNA. To further investigate the activities of this enzyme, translocation along various nucleic acid substrates was examined. Figure 7 shows a series of fluorescence time courses obtained in experiments conducted in translocation buffer at 25 °C under single-round conditions with a set of 5′ fluorescein-labeled oligo-dUs (Figure 7A) and oligo-rUs (Figure 7B) with lengths of 53, 61, and 73 nt. These data were analyzed globally using Scheme 1 (Equation (7)). The solid lines in Figure 7 are simulations using Equation (7) and the best fit parameters obtained from these analyses. The average and standard deviation of the results obtained in the analysis of at least three independent sets of experimental time courses are shown in Table 4. As shown in Table 4, the macroscopic rate of translocation for NS3h along oligo-dUs, (35.4 ± 0.6) nt/s, is ten-fold larger than the macroscopic rate of translocation for NS3h along oligo-dTs, (3.35 ± 0.09) nt/s, indicating that the macroscopic rate of NS3h translocation is dependent on the base of the nucleic acid along which it is translocating. Similarly, the macroscopic rate of translocation for NS3h along oligo-rU is approximately 1.2 fold faster than along oligo-dU, indicating a slight dependence of the macroscopic rate of translocation upon the sugar moiety of the single-stranded nucleic acid.

The results of the NLLS analysis of the three independent sets of experimental translocation time courses according to Scheme 2 (Equation (9)) are summarized in Table 4. Also included in Table 4 are the results of the analysis of the three independent sets of oligo-dTs translocation time courses according to Scheme 2 (Equation (9)). The quality of this analysis, as judged by the standard deviation of the fits, was indistinguishable from that obtained with Scheme 1 (Equation (7)) and the estimates of the macroscopic translocation rates obtained with each model are also consistent with each other.

Nucleic acid stimulated ATPase activity of NS3h

We further characterized the nucleic acid translocation activity of NS3h by measuring the kinetics of ATP consumption of NS3h during translocation along polynucleic acids. A coupled spectrophotometric assay was used to monitor the stimulation of the ATPase activity of NS3h in the presence of varying concentrations of poly(dT), poly(dU), and poly(rU). As shown in Figure 8, the ATPase activity of NS3h was stimulated in the presence of all three polynucleic acids, but the maximum stimulation was approximately 10 fold larger in the presence of poly(dU) and poly(rU) than in the presence of poly(dT). A series of experiments conducted at different ATP concentrations confirmed that a final concentration

of 1 mM ATP was saturating for NS3h in the presence of each of these nucleic acids (data not shown). The data in Figure 8A were analyzed according to Equation (11), which assumes a hyperbolic dependence of the ATPase rate on nucleic acid concentration (see Appendix). The best fit parameters obtained from this analysis are shown in Table 5 and the solid lines in Figure 8 are simulations using Equation (11) and these best fit parameters.

As shown in Table 5, the affinity of NS3h for poly(dT) is an order of magnitude tighter than the affinity of NS3h for either poly(dU) or poly(rU), and the stimulation of the ATPase rate of NS3h in the presence of either poly(dU) or poly(rU) is an order of magnitude larger than the stimulation observed in the presence of poly(dT). These results can be combined with the results of our fluorescence assay for NS3h translocation to estimate the macroscopic ATP coupling stoichiometry for nucleic acid translocation by NS3h. As shown in Table 6, we estimate that the hydrolysis of 0.5 ATP molecules are associated with the net forward translocation (from 3′ to 5′) of the NS3h monomer 1 nucleotide along the nucleic acid, regardless of which nucleic acid is the substrate for translocation or which scheme is used to analyze the kinetics of translocation; in other words, the hydrolysis of each ATP molecule is associated with a net forward translocation of 2 nt. This similarity in the estimate of the coupling efficiency suggests a common translocation mechanism for NS3h along each nucleic acid.

ITC studies of NS3h binding to short oligonucleotides

Finally, in an effort to determine the origin of the differences in the affinity of NS3h binding to $(dT)_8$, $(dU)_8$, and $(rU)_8$, we monitored the binding of NS3h to these nucleic acids using isothermal titration calorimetry. As described in Materials and Methods, we monitored the heat evolved as the oligonucleotides were titrated into a solution containing NS3h. Representative data from experiments using $(dT)_8$ and $(dU)_8$ are shown in Figure 9, panels A and B respectively. Each titration peak in Figure 9 was integrated and normalized for the amount of injectant to create the corresponding binding isotherm. The isotherms in Figure 9 were subsequently analyzed using a model that assumes a single set of sites (independent and identical) and NLLS to determine the enthalpy change ($\Delta H°$), the stoichiometry of binding (N), and equilibrium association constant (K_a) corresponding to the reaction (see Materials and Methods). The results of the analysis of the isotherms for NS3h binding to $(dT)_8$, $(dU)_8$, and $(rU)_8$ using this approach are summarized in Table 7. The estimate of a 1:1 binding stoichiometry between NS3h and these nucleic acids is consistent with the results of our sedimentation velocity experiments. These data also indicate that the binding of NS3h to each of these nucleic acids is associated with a favorable change in enthalpy and an unfavorable change in entropy, such that the binding reaction is enthalpically driven. The values of ΔH^0 and $T\Delta S^0$ associated with NS3h binding to dU_8 and rU_8 are identical, within error, but are both significantly larger (more negative) than the values of ΔH^0 and $T\Delta S^0$ associated with NS3h binding to $(dT)_8$. Finally, these data reveal that the affinity of NS3h binding is tightest for oligo-dTs and weakest for oligo-rUs, consistent with the results of our studies of the oligonucleotide stimulated ATPase activity of NS3h and the fluorescence anisotropy-based competition binding assay.

DISCUSSION

We have examined the pre-steady state kinetics of single-stranded nucleic acid translocation by monomers of the NS3 helicase from HCV using a stopped-flow fluorescence-based assay.[26; 27; 28; 31] We have found that the translocation of monomers of NS3 helicase along single-stranded nucleic acids is directionally biased from 3′ to 5′ along the nucleic acid and is coupled to the binding and hydrolysis of ATP. The time courses of nucleic acid translocation observed for NS3h monomers in our experiments are consistent with the presence of an additional process that either precedes processive nucleic acid translocation

by the monomer (Scheme 2) or is associated with the dissociation of the monomer from the 5′ end of the nucleic acid (Scheme 1). Since both models are consistent with our data, we are unable to distinguish further the validity of either. However, regardless of this uncertainty in the exact microscopic description of the kinetic mechanism of nucleic acid translocation, the estimates of the macroscopic rate of nucleic acid translocation that we obtained through a global NLLS analysis of the kinetic data are independent of the model used for the analysis.

The results of the analysis of the translocation time courses shown using either kinetic model for nucleic acid translocation demonstrate that the affinity of NS3h binding to oligo-dT is increased by approximately 12-fold by the presence of the fluorescein fluorophore (the parameter 1/r in Table 3 and Table 4). This result is consistent with the results of our experiments monitoring the equilibrium binding of NS3h to $(dT)_6$, which indicated a similar increase in the affinity of binding in the presence of the fluorophore (Table 1).

We have found that the macroscopic rate of nucleic acid translocation by NS3h monomers is dependent upon both the base and sugar moieties of the nucleic acid, with a stronger dependence observed for a change in the base. As shown in Table 3 and Table 4, the macroscopic rate of translocation for NS3h monomers along oligo-dT is an order of magnitude slower than the macroscopic rate of translocation of NS3h monomers along oligo-dU. Also, as shown in the same tables, the macroscopic rate of translocation for NS3h monomers along oligo-dU is approximately 20% slower than the macroscopic rate of translocation for NS3h monomers along oligo-rU. These estimates for the macroscopic rates of translocation are consistent with the results of our experiments characterizing the single-stranded nucleic acid stimulated ATPase activity of NS3h monomers. Our estimate of k_{cat} for NS3h monomers in the presence of poly(dU) is an order of magnitude larger than our estimate of k_{cat} for NS3h monomers in the presence of poly(dT) and our estimate of k_{cat} for NS3h monomers in the presence of poly(dU) is approximately 10% lower than our estimate of k_{cat} for NS3h monomers in the presence of poly(rU).

Based upon our estimates of the macroscopic rates of translocation and ATPase for NS3h monomers, we are able to estimate the efficiency at which NS3h couples the binding and hydrolysis of ATP to its movement along the nucleic acids. Our estimate of these efficiencies (Table 6) indicates that the binding and hydrolysis of each ATP molecule is coupled to the movement of the NS3h monomer two nucleotides along the nucleic acid, regardless of the base or sugar moiety. Interestingly, a tighter coupling of 1 ATP per nt has been suggested based upon recent crystal structures of NS3h together with single-stranded DNA and several ATP analogs.[16] In light of this discrepancy, it is worthwhile to consider the possible sources of error in our estimation of the ATP coupling stoichiometry. It is possible, for example, that we are underestimating the value of $k_{cat,\infty}$ if the lengths of poly nucleic acid used in our experiments are too short. Perhaps a slow dissociation of NS3h from the end of the nucleic acid in which no ATP is hydrolyzed is significantly contributing to the steady-state kinetics of nucleic acid translocation in those experiments. We believe that this is unlikely given the relatively low processivity of nucleic acid translocation by NS3h (Table 3 and Table 4) and the requirement that a similar large fraction of short nucleic acid molecules would be present in all three polynucleic acid samples used in our experiments. A more likely source of error might be in the estimation of the macroscopic rate of translocation. The occurrence of any process by which NS3h can move forward, from 3′ to 5′, along the nucleic acid in the absence of ATP hydrolysis would result in an overestimation in the value of the ATP coupling stoichiometry since not all the translocation events associated with our calculation of m^*k_t are directly coupled with ATP hydrolysis. Such a process might be a small slip of 1 or 2 nt or a larger jump of several nt in size. The former might result from a weakening of the interactions between the nucleic acid binding domains of NS3h and the nucleic acid, allowing for one to move relative to the other in the

absence of ATP. The latter might result from the interaction with a segment of the nucleic acid that is 5′ from NS3h and a currently uncharacterized additional nucleic acid binding site on NS3h. We would expect that were these processes to occur, their probability of occurrence would be the same for all the nucleic acids that we examined here. Indeed, although the macroscopic nucleic acid translocation rates differ for the different bases and sugars used in our experiments, the efficiency at which NS3h couples ATP binding and hydrolysis to translocation is constant for all nucleic acids. Therefore, the differences in the dependence of macroscopic rate of nucleic acid translocation by NS3h on the base and sugar moieties of the nucleic acids are independent of the differences in efficiency at which NS3h couples ATP binding and hydrolysis to nucleic acid. Instead, we propose that this difference results from the dependence of the affinity of nucleic acid binding by NS3h on the base and sugar moieties.

We observe that the affinity of nucleic acid binding is inversely correlated with the macroscopic rate of nucleic acid translocation by the NS3h monomer. This relationship exists regardless of the approach by which the affinity of nucleic acid binding is estimated (i.e., either from the value of $K_{0.5}$ determined from our analysis of the dependence of the nucleic acid stimulated ATPase rate of NS3h on nucleic acid concentration or from the estimate of ΔG^0 determined from our analysis of the binding isotherms obtained from isothermal titration calorimetry of NS3h with the nucleic acids). The tighter the NS3h monomer binds to the nucleic acid, the more slowly it translocates along it. These results suggest that the efficiency with which NS3h can couple ATP binding and hydrolysis to nucleic acid translocation provides a constraint that results in a compensatory relationship between affinity of nucleic acid binding and the macroscopic rate of nucleic acid translocation.

It is interesting to further speculate on the source of the differences in the affinity of NS3h binding to the nucleic acids in our experiments and thus on the potential structural or mechanistic origins of the relationship between binding affinity and translocation. Interpretation of the absolute values of $\Delta H°$ (and calculated $T\Delta S°$) measured in our experiments are naturally complicated by the possible contributions of linked interactions, such as proton release and subsequent proton buffer binding; nevertheless, we believe that we are justified in making comparisons between the observed thermodynamic parameters that we measured for the interaction of NS3h with the different nucleic acid substrates since these possible coupled reactions will contribute equally in each case. As shown in Table 7, the $\Delta\Delta H^0$ for NS3h binding to $(dU)_8$ versus $(dT)_8$, is equal to -7.1 ± 1.4 kcal/mol, indicating that the binding to $(dU)_8$ is enthalpically more favorable than the binding to $(dT)_8$. In view of the structural data, where the contacts between NS3h and the bound nucleic acids are limited to the sugar-phosphate backbone,[15] the differences in ΔH^0 likely result from the free energy changes within the nucleic acids themselves. Since the bound nucleic acid adopts a bent conformation when in complex with the NS3h monomer,[15] it is possible that the difference in ΔH^0 for the binding of the NS3h monomer to these nucleic acids may result from differences in the free energies associated with the reorganization of the intrinsic stacking of the bases in these nucleic acids. Indeed, the results of recent molecular dynamic simulations of thymine and uracil dimers predict that the free-energy associated with base stacking is −9.2 kcal/mol for uracil dimers and −10.8 kcal/mol for thymine dimers,[32] consistent with there being less free energy required to reorganize the base stacking inherent in $(dU)_8$ than in $(dT)_8$, and thus the binding of NS3h to $(dU)_8$ being enthalpically more favorable than the binding of NS3h to $(dT)_8$. In contrast, the binding of NS3h to $(dT)_8$ is entropically more favorable than the binding of NS3h to $(dU)_8$. Although it is more difficult to speculate on the sources of the differences in $T\Delta S^0$ for NS3h binding to these nucleic acids, possibilities may include differences in the hydration of the bases in their bound and free form [33; 34] or differences in the condensation of counter-ions around

the bases in their bound and free form.[33] Regardless, it is clear that the differences in the entropic contribution to the free energy of binding are dominantly responsible for the differences in the affinity of NS3h binding to $(dT)_8$ and $(dU)_8$.

A recently reported set of structures of NS3h bound to DNA in the presence of different ATP analogs has allowed for the development of a model for the directionally biased translocation of NS3h along DNA where intradomain structural transitions in NS3h are directly coupled to structural transitions in the DNA.[16] Specifically, the authors of this paper propose that the translocation of NS3h along the DNA is facilitated by the systematic alternation between a C2′-endo and C3′-endo conformation in the deoxyribose sugars of the DNA. In light of this model, the nucleic acid binding affinity and nucleic acid translocation activity of NS3h would be expected to be different for DNA and RNA owing to the favoring of a C3′-endo conformation by ribose due to steric hinderance of the 2′-hydroxyl group. Interestingly, although we do see a difference between the binding and translocation activities of NS3h on oligodeoxyuridylates and oligouridylates (Table 3, Table 4, Table 5, and Table 7) which may well be attributed to this preference for a C3′-endo conformation by ribose, this difference is much smaller than the differences observed between the interactions of NS3h with oligodeoxythymidylates and oligodeoxyuridylates. It is worth noting that significant rotation and bending of the DNA is also observed in these recently reported structures [16] which is consistent with the hypothesis that the free energy associated with the alterations in the base interactions of the nucleic acid significantly affect both the binding affinity of NS3h for the nucleic acid and the macroscopic rate at which NS3h can translocate along the nucleic acid.

The recently published results of a study of the DNA translocation activity of NS3 and NS3h [35] offer further support for the hypothesis that the affinity of nucleic acid binding is inversely proportional to the macroscopic rate of nucleic acid translocation. The authors of that study estimated a macroscopic translocation rate of (46 ± 5) nt/s for NS3h moving along oligodeoxythymidylates, [35] which is higher than the rate of (3.35 ± 0.09) nt/s which we estimate from our results. However, the experiments in the previous study were conducted at a higher solution NaCl concentration and at a higher temperature (50 mM NaCl vs. 30 mM NaCl and 37 °C vs. 25 °C). Since increasing the NaCl concentration and increasing the temperature would likely result in a decrease in the affinity of nucleic acid binding by NS3h, these previously published results are consistent with an inverse correlation between the macroscopic rate of translocation and the affinity of nucleic acid binding by NS3h. Of course, care must also be taken in such comparisons since the construct of NS3h used in this previous study is different from the construct of NS3h that we have used for our experiments.

The overlap between the directional bias of single-stranded nucleic acid translocation by NS3h and double-stranded nucleic acid unwinding by NS3 is consistent with single-stranded nucleic acid translocation being fundamental to double-stranded nucleic acid unwinding by this helicase.[20] This may even reflect a larger and more fundamental symmetry between single-stranded nucleic acid translocation (or tracking) and double-stranded nucleic acid unwinding for a variety of helicases.[3] Although the limitations of our analysis do not allow for an unambiguous determination of the processivity of single-stranded nucleic acid translocation by NS3h, our estimate of the processivity is nevertheless much lower than what has been reported for other helicases.[31; 36; 37] Interestingly, a recent study of single-stranded nucleic acid translocation by the ISW2 chromatin remodeling complex from *S. cerevisiae* reported a similarly low processivity for that complex. Thus, it is possible that persistent differences in the processivity (and thus also the mechanism) of nucleic acid translocation, and by extension possible differences in processivity and mechanism of double-stranded nucleic acid unwinding, may exist between the helicase families with

members of superfamily I (*E. coli* UvrD [27; 31] and *E. coli* PcrA [37]) and DNAB-like family (bacteriophage T7 helicase [36]) having higher processivities for translocation and unwinding than members of superfamily II (HCV NS3[17] and *S. cereviaise* ISW2[38]).

Despite these differences in their processivities for single-stranded nucleic acid translocation, however, helicases from across these families seem to display a similar thermodynamic efficiency with which ATP binding and hydrolysis is coupled to these activities. In this study, we estimate that the binding and hydrolysis of each ATP molecule by NS3h is coupled to the physical movement of the enzyme 2 nt along the single-stranded nucleic acid. A recent thorough study of single-stranded DNA translocation activity of monomers of the *E. coli* UvrD helicase estimated that the binding and hydrolysis of each ATP molecule was associated with the movement of the protein 1 nt along the nucleic acid. [31] Thus, differences in the processivity, and perhaps even the kinetic mechanism, of single-stranded nucleic acid translocation may be more strongly dependent upon the affinity of the translocase/helicase for the nucleic acid substrate, rather than on the physical process of energy transduction within the molecular motor itself. This hypothesis is also consistent with our observation that the differences in the macroscopic rate of translocation of NS3h along oligo-dT, oligo-dU, and oligo-rU are inversely proportional to the affinity of NS3h for those substrates, while the thermodynamic coupling efficiency of ATP binding and hydrolysis to translocation is constant for all substrates. Furthermore, we believe that the observed tight coupling between ATP binding/hydrolysis and the physical movement of the enzyme implies that the NS3h monomer has a low probability of backward motion along the nucleic acid during translocation. Because of this, we believe that our data are more consistent with a stepping (or ratchet [16]) mechanism for single-stranded nucleic acid translocation by NS3h than with a Brownian motor mechanism.[3]

In conclusion, our data indicate that the free-energy obtained from the binding and hydrolysis of a single ATP molecule is sufficient for the work required to move the NS3h monomer 2 nt along a single-stranded nucleic acid. We expect that this would also represent an upper limit for the energy transduction efficiency for double-stranded nucleic acid unwinding by the enzyme, since current models of helicase catalyzed double-stranded nucleic acid unwinding require that the helicase translocate along one strand of the duplex during unwinding.[2; 3] Indeed, the results of recent single molecule studies to probe the nucleic acid unwinding activity of NS3 are consistent with the enzyme consuming a single ATP for every base pair of nucleic acid that it unwinds. [17; 20] Taken together, these results support an active mechanism of nucleic acid unwinding by NS3 in which the free energy obtained from the binding and hydrolysis of a single ATP molecule would be partitioned into both the work required to move the enzyme along the tracking strand of the double-stranded nucleic acid and the work required to physically separate the two strands of the double-stranded nucleic acid.

MATERIALS AND METHODS

Buffers

All the buffers were prepared using reagent grade chemicals with deionized water purified by a Milli-Q purification system (Millipore Corp., Bedford, MA). The buffer (translocation buffer) used for the experiments was 25 mM MOPS (pH 7.0), 30 mM NaCl, 5 mM $MgCl_2$, 1 % (v/v) glycerol, and 2 mM DTT. The buffer was filtered with a Nalgene Filter assembly (Nalgene Nunc International, Rochester, NY) under vacuum through a filter of pore size 0.20 μm. Heparin (Sigma, St Louis, MO, catalog no. H-3393) was used at final reaction concentration of 4 mg/ml. Heparin was dialyzed extensively against Milli-Q using 3 kDa molecular mass cut-off dialysis tubing. The final concentration of the stock solution of

heparin was determined by titration with azure A, which binds to the ionizable groups on the heparin polysaccharide.[27]

DNA and RNA

Single-stranded fluorescein-labeled DNA (oligo dT and oligo dU) and RNA (oligo rU) of different lengths were purchased from TriLink Biotechnologies (San Diego, CA). Prior to use, oligonucleotides were extensively dialyzed against Milli-Q water and their concentrations were determined by spectrophotometric analysis.

Polynucleic acids were purchased from Sigma (St. Louis, MO) and Midland Certified Reagent Company Inc (Midland, TX). Polynucleic acids were dissolved and stored in nuclease free water (Ambion, Austin, TX) and their concentrations were determined by spectrophotometric analysis. For this analysis, the extinction coefficients used were rU = 8,400 M nucleotide^{-1} cm^{-1}, dU = 8,400 M nucleotide^{-1} cm^{-1}, and dT = 8,520 M nucleotide^{-1} cm^{-1}.

NS3h Cloning, Expression, and Purification

The helicase domain of the genotype 1a sequence was cloned into a modified pET28a vector which carried an rTEV cleavable 8His tag. The 5′ and 3′ primers for PCR amplification were 5′-*CATatg*agatccccggtgttcacg-3′ and 5′-*AAGCtT*TAgacgacctccaggtcggccgacatg-3′, respectively. After amplification, the PCR fragment was digested with NdeI-HindIII and gel-purified prior to ligation into the similarly cut vector DNA. In order to conform to the sequence of the published crystallized NS3h protein, S403N, L470P and T505M mutations were introduced into the helicase domain using a QuikChange Multi site-directed mutagenesis kit (Stratagene, La Jolla, CA). The final plasmid was transformed into BL21(DE3) cells. 18 L of 2xYT culture was inoculated to an A_{600nm} of 0.05 from an overnight starter culture. The culture was grown at 37 °C until an A_{600nm} of 1.0 was achieved. The culture was cooled to 28 °C and induced by the addition of 1 mM isopropyl-b-D-thiogalactopyranoside. After 3 hrs, cells were harvested by centrifugation and processed.

Cells were lysed using a Microfluidizer ® (Microfluidics, Newton, MA) with lysis buffer (25 mM HEPES pH 8.0, 10 % glycerol, 2 mM CHAPS, 0.5 M NaCl, 5 mM β-mercaptoethanol, 2 mM MgCl2, 10 mM immidazole), and the lysate was spun down using a Beckman JA25.50 rotor at 48,384 × g for 30 minutes. The supernatant was passed over a Ni-HP Hitrap column (GE Healthcare, Uppsala, Sweden) and the column was subsequently washed with lysis buffer to baseline. Protein was eluted with lysis buffer containing 0.5 M imidazole in a linear gradient of 25 column volumes (CV). Fractions containing NS3h protein were pooled and diluted fivefold with Blue Sepharose A buffer (25 mM Na-HEPES pH 8.0, 10% glycerol, 0.1% CHAPS, 5 mM DTT, 4 mM $MgCl_2$). rTEV was added at 1:15 (rTEV: NS3h) molar ratio to the diluted protein pool and incubated at 4 °C overnight. The rTEV reaction was next loaded onto a 5 ml Blue-Sepharose HP Hitrap column (GE Healthcare, Uppsala, Sweden), and the bound protein was eluted with a linear gradient of 0–1 M NaCl in Blue Sepharose A buffer over 25 CV. The Blue Sepharose pool containing His-free NS3h was diluted 5-fold with Blue Sepharose A buffer, and then loaded on the 5 ml Q Sepharose column. Protein was eluted with a linear gradient of 0–1 M NaCl in Blue Sepharose A buffer over 20 CV. The Q Sepharose pool containing NS3h was dialyzed overnight at 4 °C into 10 mM Na-Hepes, pH 7.5, 1 mM EDTA, 5 mM DTT. Protein integrity and purity was confirmed by Dynamic Light Scattering (DynaPro, Wyatt Technology Corporation, Santa Barbara, CA), Western Blot, and Mass Spectrometry (6210 Time of Flight Mass Spectrometer, Agilent Technologies, Santa Clara, CA).

Analysis of kinetic data

Unless otherwise noted, all NLLS analyses were performed using Conlin [39], kindly provided by Dr. Jeremy Williams. Fitting models and data simulation programs were written in the C computer language and compiled with the Microsoft Visual Studio.NET 2003 compiler on a Windows XP workstation. The software library CNL 6.0 (Visual Numerics Incorporated, Houston, TX) was used for the numerical calculation of the inverse Laplace transform. The uncertainties in all fitted parameters reported in this manuscript are the standard deviation of the mean.

Analytical ultracentrifugation

Dialyzed protein and DNA samples were filtered through 0.22 μm centrifugal filter devices (Ultrafree-MC, Millipore Corp., Bedford, MA) using a 5 minute centrifugation at 6,000 rpm using an Eppendorf 5414C centrifuge (Eppendorf, Hamburg, Germany) at 4 °C. Concentrations of NS3h, 5′-dT_8-Cy5-3′, and 5′-Cy5 (C6-NH) ATG TGG AAA ATC TCT AGC A-3′ were determined spectrophotometrically using calculated molar extinction coefficients of 47330 $M^{-1}cm^{-1}$ at 280 nm and 85400 $M^{-1}cm^{-1}$ and 213900 $M^{-1}cm^{-1}$ at 260 nm, respectively. Analytical sedimentation velocity experiments were performed using ProteomeLab XL-A analytical ultracentrifuge equipped with An50Ti rotor (Beckman Coulter, Fullerton, CA) at 25 °C. Absorbance data for NS3h in the absence of DNA were collected by scanning the sample cells at a wavelength of 280 nm at 42,000 rpm. The experiments performed with the Cy5 fluorophore labeled single-stranded DNA were scanned at a wavelength of 648 nm at 50,000 rpm for 5′-dT_8-Cy5-3′ and 48,000 rpm for mixed sequence 19-mer deoxyoligonucleotide. There was a small hyperchromic effect accompanying NS3h binding to the Cy5 labeled DNAs as determined from UV-VIS absorbance spectra collected for NS3h alone, DNA alone, and a few different molar ratios of NS3h to DNA.

In sedimentation velocity experiments 380 μl of samples and 392 μl of buffer were loaded into Epon charcoal-filled 2-sector centerpiece. Absorbance data were collected every 4 minutes by scanning at the selected wavelength at intervals of 0.003 cm with one average in a continuous scan mode. Continuous sedimentation coefficient distribution, c(s), was calculated using SEDFIT, which fits the sedimentations boundaries using a numerical solution to the Lamm equation.[40] In SEDFIT, the extent of diffusion for each macromolecular species is approximated with a best fitted weight-average frictional coefficient ratio for the protein mixture under study. The molar mass of macromolecules can be estimated from the best fitted values of sedimentation (s) and diffusion (D) coefficients, according to the Svedberg equation (Equation 1)[41]:

$$M = sRT / [D(1 - \bar{\upsilon}\rho)] \quad (1)$$

where M is the molecular mass; $\bar{\upsilon}$ is the partial specific volume at experimental temperature; ρ is buffer density at experimental temperature; T is an absolute temperature, R is the gas constant. Calculated s values were converted to standard conditions of water at 20 °C ($s_{20,w}$) using SEDFIT. Buffer density and viscosity were calculated from buffer composition with tabulated values in Sedenterp.[42] Weight averaged sedimentation coefficients were calculated by integration of the area under c(s) curves.[43] The frictional coefficient ratio, (f/f_o), where f is the frictional coefficient of the macromolecule under study and f_o is the frictional coefficient of a hydrated sphere of equivalent mass was calculated using Equation (2)[44; 45]:

$$\frac{f}{fo}=\left(\frac{M^2(1-\bar{\upsilon}\rho)^3}{162\pi^2(s_{20,w})^3\eta^3N_A^3(\bar{\upsilon}+\delta\upsilon^0_{H2O})}\right)^{1/3} \quad (2)$$

where η, ρ, υ^0_{H2O} are the viscosity, density and partial specific volume of pure water at 20 °C, respectively, N_A is Avogadro's number, δ is the macromolecule hydration in grams of water bound per gram of macromolecule, $\bar{\upsilon}$ is the partial specific volume of molecule at 20 °C. For NS3h $\bar{\upsilon}$ at 25 °C is equal to 0.7364 ml/g as calculated from the composition, according to the method of Cohn and Edsall[46] as implemented in Sedenterp.[42] Partial specific volumes at temperatures different that 25 °C were calculated using the relationship $\bar{\upsilon}_T = \bar{\upsilon}_{25} + 4.25E^{-4}(T - 25)$.[47] The value of the partial specific volume for 5′-dT_8-Cy5-3′ and 5′-Cy5-18-mer-3′ was assumed to be equal to 0.61 ml/g and 0.58 ml/g, respectively based upon previously reported values for $(dT)_n$, $(dA)_n$, $(dC)_n$, $(dG)_n$ [48]

In *f*/*fo* calculations, an estimated value of degree of hydration for NS3h equal to δ = 0.2628 g of water bound per gram of protein was used. This value was calculated based on the amino acid sequence of NS3h using the Kuntz[49] method as implemented in Sedenterp and with the correction of Lin *et al*.,[50] which takes into account that only around 70 % of water molecules calculated by Kuntz's method seem to be associated with folded proteins. For 5′-dT_8-Cy5-3′ and 5′-Cy5-19-mer-3′, a value of δ = 0.434 g of water bound per gram of DNA was used.[51]

The weight average, $\bar{\upsilon}$, for the NS3h-DNA complex at 20°C was calculated from $\bar{\upsilon}$ and molar masses of individual components (M_{NS3h} = 48637.73 g/mol, $M_{5'\text{-dT8-Cy5-3}'}$ = 3189.6 g/mol, $M_{5'\text{-Cy5-19-mer}}$ = 6655.8 g/mol) according to Equation (3)[46] and is equal to $\bar{\upsilon}_{NS3h\text{-dT8}}$ = 0.7266 ml/g and $\bar{\upsilon}_{NS3h\text{-}5'\text{-Cy5-19-mer}}$ = 0.7156 ml/g.

$$\bar{\upsilon}=\left(\sum_{i=1}^{n}n_iM_i\bar{\upsilon}_i\right)/\left(\sum_{i=1}^{n}n_iM_i\right) \quad (3)$$

Fluorescence Anisotropy Based Assay for Binding of NS3 to fluorescently labeled oligonucleotides

Experiments monitoring the binding of NS3h to polynucleic acids were performed in translocation buffer with an additional 0.1 mg/ml BSA at 25 °C using a fluorescence anisotropy based assay. In this assay, 5 nM of fluorescently labeled deoxyoligonucleotide 5′-F-dT_6 or 5′-dT_6-F was titrated with increasing concentrations of helicase domain (0 μM to 5 μM). After 35 minutes of incubation at room temperature, the fluorescence anisotropy was measured at 25 °C using a Safire2 microplate reader (Tecan Group Ltd., Mannedorf, Switzerland). The resulting binding isotherms were fit to Equation (4) to determine an estimate of the equilibrium dissociation constant, K_d, for the interaction of NS3h with the DNA.

$$r=\frac{f_B(r_F-Rr_B)-r_F}{f_B(1-R)-1} \quad (4)$$

Equation (4) was obtained upon rearrangement of formula for the fraction of bound fluorescent oligonucleotode – f_B- in the case where there is a change in fluorescence

intensity upon formation of protein-oligonucleotide complex [52]; [53]. In Equation (4), r is measured fluorescence anisotropy of the fluorescently labeled deoxyoligonucleotide, r_F and r_B are the anisotropies of the free and bound oligonucleotide, respectively and $R = F_B/F_F$ is the ratio of fluorescence intensities of the free and bound forms. Taking into account a simple 1:1 binding model, the fraction of bound fluorescent oligonucleotode can be expressed with Equation (5)

$$f_B = \frac{(1/K_d) * [X_f])}{1+(1/K_d) * [X_f]} \quad (5)$$

where $[X_f] = [X_T]/(1+ (1/K_d) *[M_f])$ is the concentration of free NS3h; $[M_f] = [M_T]/(1+ (1/K_d) *[X_f])$ is the concentration of free fluorophore labeled $dT_{6;}$. $[X_T]$, $[M_T]$ are the total concentrations of NS3h and fluorophore labeled dT_6, respectively. The implicit fitting of the binding isotherms shown in Figure 3A using Equation (4) and Equation (5) was performed with the Scientist software package (Micromath, St. Louis, MO).

Competition Fluorescence Anisotropy Based Assay for Binding of NS3 to unlabeled oligonucleotides

The equilibrium dissociation constant for interaction of NS3h with unlabeled deoxyoligonucleotide was determined using a competition binding assay based on measurements of fluorescence anisotropy of fluorescently labeled deoxyoligonucleotide 5′-F-dT_6 or 5′-dT_6-F as a probe. The concentrations of fluorescently labeled deoxyoligonucleotide and protein were kept constant at 5 nM and 100 nM, respectively, in experiments with 5′-F-dT_6 or at 5 nM and 500 nM, respectively, in experiments with 5′-dT_6-F. In this assay, aliquots of NS3h were added to a solution containing a mixture of fluorescently labeled $(dT)_6$ and increasing concentrations of unlabeled competitor (0 μM to 50 μM). After 35 minutes of incubation at room temperature, the fluorescence anisotropy was measured at 25 °C using the Safire2 microplate reader (Tecan Group Ltd., Mannedorf, Switzerland). The resulting binding isotherms were analyzed using Equation (4) and Equation (5) and taking into account simple equilibrium binding model that assumes competitive binding between the probe and competitor molecules in calculation of fraction of free species. Therefore, $[X_f] = [X_T]/(1+ (1/K_d) *[M_f] + (1/K_i) * D_f)$ is the concentration of free NS3h; $[M_f] = [M_T]/(1+ (1/K_d) *[X_f])$ is the concentration of free fluorophore labeled $dT_{6;}$ and $[D_f] = [D_T]/(1+ (1/K_i) *[X_f])$ is the concentration of free unlabeled competitor. $[X_T]$, $[M_T]$ and $[D_T]$ are the total concentrations of NS3h, fluorophore labeled dT_6 and unlabeled competitor oligonucleotide, respectively. In the analysis of the binding isotherms shown in Figure 3B using Equation (4) and Equation (5) the value of K_d, the affinity of NS3h binding to the fluorophore labeled oligodeoxynucleotide, was constrained to the average value obtained in the independent experiments described above and shown in Table 1. The implicit fitting of the binding isotherms shown in Figure 3B was performed with the Scientist software package (Micromath, St. Louis, MO) and returned estimates of the equilibrium dissociation constant, K_i, for the binding of NS3h to the competitor molecule.

Fluorescence stopped-flow experiments

All fluorescence stopped-flow experiments were carried out in translocation buffer at 25 °C using an Applied Photophysics SX.18MV-R Stopped-Flow Spectrophotometer (Applied Photophysics Ltd., Leatherhead, UK). Optical filters were purchased from ThorLabs (Newton, N.J.). The fluorescein fluorophore was excited at 492 nm and its fluorescence emission was monitored at wavelengths > 520 nm using a long-pass filter. The Cy3 fluorophore was excited at 550 nm and its fluorescence emission was monitored at

wavelengths > 570 nm using a long-pass filter. NS3h (200 nM) was incubated with either DNA or RNA (400 nM) at 4 °C for 5 minutes before loading onto one of the syringes of the stopped flow instrument. These experiments were performed under conditions where the total concentration of the DNA was in excess of the total concentration of NS3h to ensure that the only bound species where NS3h monomers.[27; 28] The solution of 10 mM $MgCl_2$, 2 mM ATP and 8 mg/ml heparin was loaded on the other syringe of the stopped flow. Reaction mixtures in both syringes were incubated for 2 minutes at 25°C to allow for temperature equilibration prior to mixing. Following the 1:1 mixing of the two solutions, the final reaction concentrations were: 100 nM NS3h, 200 nM DNA or RNA, 1 mM ATP, 5 mM $MgCl_2$, and 4 mg/ml heparin. The kinetic traces used for analysis are an average of at least 10 individual traces.

Equations for Analysis of Kinetic Translocation Data

The expression for fluorophore fluorescence associated with Scheme 1 is shown in Equation (6).

$$f(t)=L^{-1}\left[\frac{A}{((n-1)*r+rn+1)(k_d+s)(k_{end,1}+k_2+s)}\left(1+BA\frac{k_{end,1}}{k_{end,2}+s}\right)\left(k_d+k_t*r+s-\left(\frac{k_t}{k_t+k_d+s}\right)^n(k_t*r+(r-rn)(k_d+s))\right)\right] \quad (6)$$

In this equation, L^{-1} is the inverse Laplace transform operator, s is the Laplace variable, k_t, k_d, k_c, k_{end}, and n are as defined in the results. The variable A is a scalar factor incorporating both the initial concentration of protein bound to the single-stranded oligonucleotide and the fluorescence signal change associated with protein being bound at the 5′ end of the DNA (in the T_0 state in Scheme 1). The variable BA is the ratio of the fluorescence signal change associated with an NS3h monomer completing the second step of the two step dissociation process from the 5′ end of the oligonucleotide to the fluorescence signal change associated with the NS3h monomer being bound at the 5′ end of the DNA. The variable r is the ratio of the initial probability (before the addition of ATP) of the enzyme being bound to any other position (other than the 3′ or 5′ ends) on the single-stranded oligonucleotide to the initial probability of the NS3h monomer being bound to 5′ end of the DNA.[28] The variable rn is the ratio of the initial probability (before the addition of ATP) of the enzyme being bound to the 3′ end of the single-stranded oligonucleotide to the initial probability of the NS3h monomer being bound to 5′ end of the oligonucleotide. Because the parameter $k_{end,1}$ appears either in summation with k_2 or as a product with BA, it is not possible to determine a value for it. Instead, we are limited to determining the sum of $k_{end,1}$ and k_2. Because of this, we used a simplified version of Equation (6), shown in Equation (7) for the analysis of the kinetic time courses.

$$f(t)=L^{-1}\left[\frac{A}{((n-1)*r+rn+1)(k_d+s)(k_{end,1}+k_2+s)}\left(1+\frac{BA}{k_{end,2}+s}\right)\left(k_d+k_t*r+s-\left(\frac{k_t}{k_t+k_d+s}\right)^n(k_t*r+(r-rn)(k_d+s))\right)\right] \quad (7)$$

The expression for fluorophore fluorescence associated with Scheme 2 is shown in Equation 8.

$$f(t)=L^{-1}\left[\frac{A}{((n-1)*r+rn+1)(k_i+k_2+s)}\left(BA+\frac{k_i\left(k_d+k_t*r+s-\left(\frac{k_t}{k_t+k_d+s}\right)^n(k_t*r+(r-rn)(k_d+s))\right)}{(k_d+s)(k_{end}+s)}\right)\right] \quad (8)$$

Because an estimate of the parameter k_i can not be determined independent of its summation with the parameter k_2, we use a simplified version of Equation (8), shown in Equation (9) for the analysis of the kinetic time courses.

$$f(t)=L^{-1}\left[\frac{A}{((n-1)*r+rn+1)(k_i+k_2+s)}\left(BA+\frac{\left(k_d+k_t*r+s-\left(\frac{k_t}{k_t+k_d+s}\right)^n(k_t*r+(r-rn)(k_d+s))\right)}{(k_d+s)(k_{end}+s)}\right)\right] \quad (9)$$

As shown in Equation (10), we can relate n to the kinetic step size of translocation, m, and the interaction size of the NS3h monomer on the DNA, d.[27; 28; 31].

$$n=\frac{L-d}{m} \quad (10)$$

In the global analysis of kinetic time courses using Equation (10) and either Equation (7) or Equation (9), the values of k_t, k_d, r, $k_{end,1}$, $k_{end,2}$, k_i, m, d, and BA were constrained to be global parameters (independent of the length of the oligonucleotide), whereas the value of A was allowed to be different for each length of oligonucleotide.

ATPase Assay

All experiments were carried out at 25 °C in translocation buffer with 5 mM KCl and 1 mM $MgCl_2$. ATPase assays were carried out utilizing the PK-LDH coupled system. Briefly, nucleic acid solutions were assembled in nuclease free water and prepared through a series of two-fold dilutions from 1 mM nucleotide (poly(rU), poly(dU)) or 250 μM nucleotide (poly(dT)) down to 977 nM nucleotide and 244 nM nucleotide, respectively. Titrated nucleic acid (poly(rU), poly(dU), poly(dT)) was mixed with NS3h (70 nM), NADH (0.4 mg/ml), pyruvate kinase (3.5 U/ml), and lactate dehydrogenase (5 U/ml) in a Costar 96-well round-bottom polystyrene plate (#3795, Corning Inc., Corning, NY). ATP (1 mM) and phosphoenol pyruvate (0.31 mg/ml) were added to initiate the reaction. After shaking the plate for 10 seconds to mix, the reaction progress was monitored at an absorbance of 340 nm on a Biotek Synergy2 plate reader (BioTek Instruments, Inc., Winooski, VT) for 15 minutes (1 read every 30 seconds). Finally, initial rates were extracted from the slope determined from a linear fit of the initial linear phase of the kinetic data and converted from absorbance-based units (OD/s) to concentration-based units ([μM ADP produced]/s) using an ADP standard curve.

The dependence of the ATPase rate on poly nucleic acid concentration was analyzed using the hyperbolic function shown in Equation (11).

$$\frac{\text{ATPase rate}}{[NS3h]_{total}}=k_o+k_{cat}\left(\frac{[\text{nucleic acid}]}{[\text{nucleic acid}]+K_{0.5}}\right) \quad (11)$$

In Equation (11), k_0 is the basal ATPase rate of NS3h in the absence of nucleic acid; k_{cat} is the maximum ATPase rate under saturating concentrations of nucleic acid; and $K_{0.5}$ is the concentration of nucleic acid required to achieve ½ of the maximum ATPase stimulation. See appendix for a derivation of Equation (11).

Isothermal Calorimetry

The NS3h protein was dialyzed against 2 L of titration buffer (25 mM MOPS pH 7.0, 30 mM NaCl, 5 mM $MgCl_2$, 1 mM TCEP, 1 % Glycerol), and clarified using a 0.22 μm syringe filter post dialysis. Protein concentration was determined spectrophotmetrically using an extinction coefficient ε_{280} of 47324.3 $M^{-1}cm^{-1}$. Oligonucleotides were stored in water and stock concentrations were determined using extinction coefficients ε_{260} of 77800 $M^{-1}cm^{-1}$ for $dU_8$and rU_8, and 65400 $M^{-1}cm^{-1}$ for dT_8. Reagents were prepared for ITC experiments using the dialysis buffer to dilute to the appropriate concentration of ~10 μM for the protein to be placed in the cell; and ~100 μM for the oligonucleotides to be placed in the syringe. All solutions were degassed prior to loading into the ITC instrument; after which the concentration of all components was determined using absorbance measurements. Syringe solutions were titrated into the cell in 10 μL increments with 240 seconds between each injection with a total of 29 injections. An initial 3 μL injection was performed and discarded from analysis. All experiments were performed using a VP-ITC instrument (Microcal, Northampton, MA) at 25 °C with a stirring speed of 490 RPM. Each analysis was performed in duplicate and additional control experiments were performed including titration of the oligonucleotides into buffer to measure heat of dilution effects. Data was processed and analyzed using Origin software package as provided by Microcal. Each titration peak was integrated to determine the heat released during injection and normalized per mole of injected ligand. The subsequent binding isotherms were corrected for heat of dilution using reference titrations of the ligand into the buffer and fit to a N independent and identical binding sites model using NLLS analysis to determine estimates of the stoichiometry of the association, the association constant (K_a) and the enthalpy of binding ($\Delta H°$) for the binding equilibrium. The free energy of binding ($\Delta G°$) and the entropic contribution was determined using equation (12).

$$\Delta G^o = -RT\ln K_a = \Delta H^o - T\Delta S^o \quad (12)$$

In Equation (12), R is the universal gas constant and T is the absolute temperature. Parameters from duplicate experiments were averaged and a standard deviation determined.

Acknowledgments

The authors wish to thank Dr. Alex Kozlov for careful reading of the manuscript and help with the interpretation of the binding and isothermal titration calorimetry data. We would also like to thank Dr. Joy Feng for careful reading of the manuscript and discussion. This work was supported by NIH grant P20 RR017708.

Abbreviations

NLLS non-linear least squares

References

1. LOHMAN TM, BJORNSON KP. MECHANISMS OF HELICASE-CATALYZED DNA UNWINDING. ANNU REV BIOCHEM. 1996; 65:169–214. [PubMed: 8811178]

2. LOHMAN TM, TOMKO EJ, WU CG. NON-HEXAMERIC DNA HELICASES AND TRANSLOCASES: MECHANISMS AND REGULATION. NAT REV MOL CELL BIOL. 2008; 9:391–401. [PubMed: 18414490]

3. PATEL SS, DONMEZ I. MECHANISMS OF HELICASES. J BIOL CHEM. 2006; 281:18265–8. [PubMed: 16670085]

4. PYLE AM. TRANSLOCATION AND UNWINDING MECHANISMS OF RNA AND DNA HELICASES. ANNU REV BIOPHYS. 2008; 37:317–36. [PubMed: 18573084]

5. SINGLETON MR, DILLINGHAM MS, WIGLEY DB. STRUCTURE AND MECHANISM OF HELICASES AND NUCLEIC ACID TRANSLOCASES. ANNU REV BIOCHEM. 2007; 76:23–50. [PubMed: 17506634]

6. DELAGOUTTE E, VON HIPPEL PH. HELICASE MECHANISMS AND THE COUPLING OF HELICASES WITHIN MACROMOLECULAR MACHINES. PART II: INTEGRATION OF HELICASES INTO CELLULAR PROCESSES. Q REV BIOPHYS. 2003; 36:1–69. [PubMed: 12643042]

7. LOHMAN, TM.; HSIEH, J.; MALUF, NK.; CHENG, W.; LUCIUS, AL.; FISCHER, CJ.; BRENDZA, KM.; KOROLEV, S.; WAKSMAN, G. DNA HELICASES, MOTORS THAT MOVE ALONG NUCLEIC ACIDS: LESSONS FROM THE SF1 HELICASE SUPERFAMILY. HACKNEY, DD.; TAMANOI, F., editors. THE ENZYMES; 2003.

8. BARTENSCHLAGER R, LOHMANN V. REPLICATION OF HEPATITIS C VIRUS. J GEN VIROL. 2000; 81:1631–48. [PubMed: 10859368]

9. KIM DW, GWACK Y, HAN JH, CHOE J. C-TERMINAL DOMAIN OF THE HEPATITIS C VIRUS NS3 PROTEIN CONTAINS AN RNA HELICASE ACTIVITY. BIOCHEM BIOPHYS RES COMMUN. 1995; 215:160–6. [PubMed: 7575585]

10. SUZICH JA, TAMURA JK, PALMER-HILL F, WARRENER P, GRAKOUI A, RICE CM, FEINSTONE SM, COLLETT MS. HEPATITIS C VIRUS NS3 PROTEIN POLYNUCLEOTIDE-STIMULATED NUCLEOSIDE TRIPHOSPHATASE AND COMPARISON WITH THE RELATED PESTIVIRUS AND FLAVIVIRUS ENZYMES. J VIROL. 1993; 67:6152–8. [PubMed: 8396675]

11. KOLYKHALOV AA, MIHALIK K, FEINSTONE SM, RICE CM. HEPATITIS C VIRUS-ENCODED ENZYMATIC ACTIVITIES AND CONSERVED RNA ELEMENTS IN THE 3′ NONTRANSLATED REGION ARE ESSENTIAL FOR VIRUS REPLICATION IN VIVO. J VIROL. 2000; 74:2046–51. [PubMed: 10644379]

12. TAI CL, CHI WK, CHEN DS, HWANG LH. THE HELICASE ACTIVITY ASSOCIATED WITH HEPATITIS C VIRUS NONSTRUCTURAL PROTEIN 3 (NS3). J VIROL. 1996; 70:8477–84. [PubMed: 8970970]

13. PANG PS, JANKOWSKY E, PLANET PJ, PYLE AM. THE HEPATITIS C VIRAL NS3 PROTEIN IS A PROCESSIVE DNA HELICASE WITH COFACTOR ENHANCED RNA UNWINDING. EMBO J. 2002; 21:1168–76. [PubMed: 11867545]

14. MATLOCK DL, YERUVA L, BYRD AK, MACKINTOSH SG, LANGSTON C, BROWN C, CAMERON CE, FISCHER CJ, RANEY KD. INVESTIGATION OF TRANSLOCATION, DNA UNWINDING, AND PROTEIN DISPLACEMENT BY NS3H, THE HELICASE DOMAIN FROM THE HEPATITIS C VIRUS HELICASE. BIOCHEMISTRY.

15. KIM JL, MORGENSTERN KA, GRIFFITH JP, DWYER MD, THOMSON JA, MURCKO MA, LIN C, CARON PR. HEPATITIS C VIRUS NS3 RNA HELICASE DOMAIN WITH A BOUND OLIGONUCLEOTIDE: THE CRYSTAL STRUCTURE PROVIDES INSIGHTS INTO THE MODE OF UNWINDING. STRUCTURE. 1998; 6:89–100. [PubMed: 9493270]

16. GU M, RICE CM. THREE CONFORMATIONAL SNAPSHOTS OF THE HEPATITIS C VIRUS NS3 HELICASE REVEAL A RATCHET TRANSLOCATION MECHANISM. PROC NATL ACAD SCI U S A. 107:521–8. [PubMed: 20080715]

17. DUMONT S, CHENG W, SEREBROV V, BERAN RK, TINOCO I JR, PYLE AM, BUSTAMANTE C. RNA TRANSLOCATION AND UNWINDING MECHANISM OF HCV NS3 HELICASE AND ITS COORDINATION BY ATP. NATURE. 2006; 439:105–8. [PubMed: 16397502]

18. LEVIN MK, GURJAR M, PATEL SS. A BROWNIAN MOTOR MECHANISM OF TRANSLOCATION AND STRAND SEPARATION BY HEPATITIS C VIRUS HELICASE. NAT STRUCT MOL BIOL. 2005; 12:429–35. [PubMed: 15806107]
19. LEVIN MK, GURJAR MM, PATEL SS. ATP BINDING MODULATES THE NUCLEIC ACID AFFINITY OF HEPATITIS C VIRUS HELICASE. J BIOL CHEM. 2003; 278:23311–6. [PubMed: 12660239]
20. MYONG S, BRUNO MM, PYLE AM, HA T. SPRING-LOADED MECHANISM OF DNA UNWINDING BY HEPATITIS C VIRUS NS3 HELICASE. SCIENCE. 2007; 317:513–6. [PubMed: 17656723]
21. SEREBROV V, PYLE AM. PERIODIC CYCLES OF RNA UNWINDING AND PAUSING BY HEPATITIS C VIRUS NS3 HELICASE. NATURE. 2004; 430:476–80. [PubMed: 15269774]
22. SOULTANAS P, DILLINGHAM MS, WILEY P, WEBB MR, WIGLEY DB. UNCOUPLING DNA TRANSLOCATION AND HELICASE ACTIVITY IN PCRA: DIRECT EVIDENCE FOR AN ACTIVE MECHANISM. EMBO J. 2000; 19:3799–810. [PubMed: 10899133]
23. SOULTANAS P, WIGLEY DB. UNWINDING THE ‘GORDIAN KNOT’ OF HELICASE ACTION. TRENDS BIOCHEM SCI. 2001; 26:47–54. [PubMed: 11165517]
24. YU J, HA T, SCHULTEN K. HOW DIRECTIONAL TRANSLOCATION IS REGULATED IN A DNA HELICASE MOTOR. BIOPHYS J. 2007; 93:3783–97. [PubMed: 17704159]
25. BERAN RK, BRUNO MM, BOWERS HA, JANKOWSKY E, PYLE AM. ROBUST TRANSLOCATION ALONG A MOLECULAR MONORAIL: THE NS3 HELICASE FROM HEPATITIS C VIRUS TRAVERSES UNUSUALLY LARGE DISRUPTIONS IN ITS TRACK. J MOL BIOL. 2006; 358:974–82. [PubMed: 16569413]
26. DILLINGHAM MS, WIGLEY DB, WEBB MR. DIRECT MEASUREMENT OF SINGLE-STRANDED DNA TRANSLOCATION BY PCRA HELICASE USING THE FLUORESCENT BASE ANALOGUE 2-AMINOPURINE. BIOCHEMISTRY. 2002; 41:643–51. [PubMed: 11781105]
27. FISCHER CJ, MALUF NK, LOHMAN TM. MECHANISM OF ATP-DEPENDENT TRANSLOCATION OF E. COLI UVRD MONOMERS ALONG SINGLE-STRANDED DNA. J MOL BIOL. 2004; 344:1287–309. [PubMed: 15561144]
28. FISCHER CJ, LOHMAN TM. ATP-DEPENDENT TRANSLOCATION OF PROTEINS ALONG SINGLE-STRANDED DNA: MODELS AND METHODS OF ANALYSIS OF PRE-STEADY STATE KINETICS. J MOL BIOL. 2004; 344:1265–86. [PubMed: 15561143]
29. ZHANG W, BOND JP, ANDERSON CF, LOHMAN TM, RECORD MT JR. LARGE ELECTROSTATIC DIFFERENCES IN THE BINDING THERMODYNAMICS OF A CATIONIC PEPTIDE TO OLIGOMERIC AND POLYMERIC DNA. PROC NATL ACAD SCI U S A. 1996; 93:2511–6. [PubMed: 8637905]
30. ZHANG W, NI H, CAPP MW, ANDERSON CF, LOHMAN TM, RECORD MT JR. THE IMPORTANCE OF COULOMBIC END EFFECTS: EXPERIMENTAL CHARACTERIZATION OF THE EFFECTS OF OLIGONUCLEOTIDE FLANKING CHARGES ON THE STRENGTH AND SALT DEPENDENCE OF OLIGOCATION (L8+) BINDING TO SINGLE-STRANDED DNA OLIGOMERS. BIOPHYS J. 1999; 76:1008–17. [PubMed: 9916032]
31. TOMKO EJ, FISCHER CJ, NIEDZIELA-MAJKA A, LOHMAN TM. A NONUNIFORM STEPPING MECHANISM FOR E. COLI UVRD MONOMER TRANSLOCATION ALONG SINGLE-STRANDED DNA. MOL CELL. 2007; 26:335–47. [PubMed: 17499041]
32. GU J, WANG J, LESZCZYNSKI J, XIE Y, SCHAEFER HF. TO STACK OR NOT TO STACK: PERFORMANCE OF A NEW DENSITY FUNCTIONAL FOR THE URACIL AND THYMINE DIMERS. CHEMICAL PHYSICS LETTERS. 2008; 459:164–166.
33. OLSEN CM, MARKY LA. ENERGETIC AND HYDRATION CONTRIBUTIONS OF THE REMOVAL OF METHYL GROUPS FROM THYMINE TO FORM URACIL IN G-QUADRUPLEXES. THE JOURNAL OF PHYSICAL CHEMISTRY B. 2009; 113:9–11. [PubMed: 19198041]
34. SAITO M, SARAI A. FREE ENERGY CALCULATIONS FOR THE RELATIVE BINDING AFFINITY BETWEEN DNA AND LAMDA-REPRESSOR. PROTEINS: STRUCTURE, FUNCTION AND GENETICS. 2003; 52:129–136.

35. MATLOCK DL, YERUVA L, BYRD AK, MACKINTOSH SG, LANGSTON C, BROWN C, CAMERON CE, FISCHER CJ, RANEY KD. INVESTIGATION OF TRANSLOCATION, DNA UNWINDING, AND PROTEIN DISPLACEMENT BY NS3H, THE HELICASE DOMAIN FROM THE HEPATITIS C VIRUS HELICASE. BIOCHEMISTRY. 2010; 49:2097–109. [PubMed: 20108974]
36. KIM DE, NARAYAN M, PATEL SS. T7 DNA HELICASE: A MOLECULAR MOTOR THAT PROCESSIVELY AND UNIDIRECTIONALLY TRANSLOCATES ALONG SINGLE-STRANDED DNA. J MOL BIOL. 2002; 321:807–19. [PubMed: 12206763]
37. NIEDZIELA-MAJKA A, CHESNIK MA, TOMKO EJ, LOHMAN TM. BACILLUS STEAROTHERMOPHILUS PCRA MONOMER IS A SINGLE-STRANDED DNA TRANSLOCASE BUT NOT A PROCESSIVE HELICASE IN VITRO. J BIOL CHEM. 2007; 282:27076–85. [PubMed: 17631491]
38. FISCHER CJ, YAMADA K, FITZGERALD DJ. KINETIC MECHANISM FOR SINGLE STRANDED DNA BINDING AND TRANSLOCATION BY *S. CEREVISIAE* ISW2. BIOCHEMISTRY. 2009; 48:2960–2968. [PubMed: 19203228]
39. WILLIAMS DJ, HALL KB. MONTE CARLO APPLICATIONS TO THERMAL AND CHEMICAL DENATURATION EXPERIMENTS OF NUCLEIC ACIDS AND PROTEINS. METHODS ENZYMOL. 2000; 321:330–52. [PubMed: 10909065]
40. DAM J, SCHUCK P. CALCULATING SEDIMENTATION COEFFICIENT DISTRIBUTIONS BY DIRECT MODELING OF SEDIMENTATION VELOCITY CONCENTRATION PROFILES. METHODS IN ENZYMOLOGY. 2004; 384:185–212. [PubMed: 15081688]
41. SVEDBERG, T. THE ULTRACENTRIFUGE. JOHNSON REPRINT CORPORATION; NEW YORK: 1940.
42. LAUE, TM.; SHAH, BD.; RIDGEWAY, TM.; PELLETIER, SL. ANALYTICAL ULTRACENTRIFUGATION IN BIOCHEMISTRY AND POLYMER SCIENCE. ROYAL SOCIETY OF CHEMISTRY; CAMBRIDGE: 1992. COMPUTER-AIDED INTERPRETATION OF ANALYTICAL SEDIMENTATION DATA FOR PROTEINS.
43. SCHUCK, P. DIFUSION-DECONVOLUTED SEDIMENTATION COEFFICIENT DISTRIBUTIONS FOR THE ANALYSIS OF INTERACTING AND NON-INTERACTING PROTEIN MIXTURES. ANALYTICAL ULTRACENTRIFUGATION. In: SCOTT, DJ.; HARDING, SE.; ROWE, AJ., editors. ANALYTICAL ULTRACENTRIFUGATION TECHNIQUES AND METHODS. THE ROYAL SOCIETY OF CHEMISTRY; CAMBRIDGE: 2005.
44. BUJALOWSKI W, KLONOWSKA MM, JEZEWSKA MJ. OLIGOMERIC STRUCTURE OF ESCHERICHIA COLI PRIMARY REPLICATIVE HELICASE DNAB PROTEIN. JOURNAL OF BIOLOGICAL CHEMISTRY. 1994; 269:31350–31358. [PubMed: 7989299]
45. TANFORD, C. PHYSICAL CHEMISTRY OF MACROMOLECULES. WILEY; NEW YORK: 1961.
46. COHN, EJ.; EDSTAL, JT. PROTEINS, AMINO ACIDS AND PEPTIDES AS IONS AND DIPOLAR IONS. RHEINHOLD; NEW YORK: 1943.
47. DURCHSCHLAG, H.; HINZ, H-J., editors. THERMODYNAMIC DATA FOR BIOCHEMISTRY AND BIOTECHNOLOGY. NEW YORK: SPRINGER-VERLAG; 1986. SPECIFIC VOLUMES OF BIOLOGICAL MACROMOLECULES AND SOME OTHER MOLECULES OF BIOLOGICAL INTEREST.
48. HATTERS DM, WILSON L, ATCLIFFE BW, MULHERN TD, GUZZO-PERNELL N, HOWLETT GJ. SEDIMENTATION ANALYSIS OF NOVEL DNA STRUCTURES FORMED BY HOMO-OLIGONUCLEOTIDES. BIOPHYS J. 2001; 81:371–81. [PubMed: 11423421]
49. KUNTZ ID JR. HYDRATION OF MACROMOLECULES. IV. POLYPEPTIDE CONFORMATION IN FROZEN SOLUTIONS. JOURNAL OF THE AMERICAN CHEMICAL SOCIETY. 1971; 93:516–518. [PubMed: 5541519]
50. LIN TH, QUINN T, WALSH M, GRANDGENETT D, LEE JC. AVIAN MYELOBLASTOSIS VIRUS REVERSE TRANSCRIPTASE. EFFECT OF GLYCEROL ON ITS HYDRODYNAMIC PROPERTIES. JOURNAL OF BIOLOGICAL CHEMISTRY. 1991; 266:1635–1640. [PubMed: 1703151]

51. BASTOS M, CASTRO V, MREVLISHVILI G, TEIXEIRA J. HYDRATION OF DS-DNA AND SS-DNA BY NEUTRON QUASIELASTIC SCATTERING. BIOPHYSICAL JOURNAL. 2004; 86:3822–3827. [PubMed: 15189878]

52. BUJALOWSKI W, LOHMAN TM. MONOMER-TETRAMER EQUILIBRIUM OF THE ESCHERICHIA COLI SSB-1 MUTANT SINGLE STRAND BINDING PROTEIN. J BIOL CHEM. 1991; 266:1616–26. [PubMed: 1988441]

53. MALENCIK DA, ANDERSON SR. PEPTIDE BINDING BY CALMODULIN AND ITS PROTEOLYTIC FRAGMENTS AND BY TROPONIN C. BIOCHEMISTRY. 1984; 23:2420–8. [PubMed: 6148100]

Appendix: Translocation Models

I. Simple Translocation Model

A simple model for steady-state translocation of NS3h along a single-stranded nucleic acid is depicted in Scheme A1. In this model, a monomer of NS3h with a contact size of *d* nucleotides binds with polarity to a single-stranded-nucleic acid, *L* nucleotides long. The NS3h monomer is initially bound *i* translocation steps away from the 5′ end of the nucleic acid, with concentration $[T_i]$; the number of translocation steps, *i*, is constrained ($0 \le i \le n$), where *n* is the maximum number of translocation steps needed for a monomer of NS3h initially bound at the 3′ end of the nucleic acid to translocate to the 5′ end of the nucleic acid. In this model we assume that the binding of the NS3h monomers to the single-stranded nucleic acid is random, but uniform, so that there is an equal probability of binding to any position along the nucleic acid.

Upon addition of ATP, the translocase moves with directional bias along the DNA via a series of repeated rate-limiting translocation steps each associated with the same rate constant, k_t. The rate constant for protein dissociation during translocation is k_d. The processivity of translocation along the DNA is defined as $P=\frac{k_t}{k_d+k_t}$. Between two successive rate-limiting translocation steps the protein moves *m* nucleotides, while hydrolyzing *c* ATP molecules. Therefore, *c/m* is defined as the macroscopic ATP coupling stoichiometry and corresponds to the average number of ATP molecules hydrolyzed per nucleotide translocated along the single-stranded nucleic acid. Similarly the product m^*k_t is the macroscopic translocation rate and has units of nucleotides/s. The kinetic step size of translocation, *m*, is related to the length, *L*, and maximum number of translocation steps, *n*, of a given nucleic acid through equation (A1).

$$m=\frac{L-d}{n} \tag{A1}$$

Any NS3h monomers that dissociate from the nucleic acid during translocation, or that were initially free in solution, can bind the nucleic acid at any position. We assume that the concentration of the nucleic acid is sufficiently high so that we can treat the binding of NS3h to the nucleic acid as a pseudo-first-order process with an associated pseudo-first-order rate constant, k_b*[NA], where [NA] is the concentration of the nucleic acid and k_b is the bi-molecular rate constant for NS3h binding to the nucleic acid.

The differential equations associated with the concentration of NS3h monomers at a specific position, *i*, along a nucleic acid with *n* maximum translocation steps (denoted as $\left[T_i^n\right]$) can be

solved to determine expressions for the time dependence of the concentration of NS3h monomers at this position, $\left[T_i^n(t)\right]$. These expressions are given in Equations (A2) and (A3).

$$L\left\{\frac{\left[T_{i\neq 0}^n(t)\right]}{[NS3h]_{total}}\right\}=\frac{(k_b[NA]+s)}{s(n+1)(k_b[NA]+k_d+s)}\left(1-\left(\frac{k_t}{k_t+k_d+s}\right)^{1-i+n}\right) \tag{A2}$$

$$L\left\{\frac{\left[T_0^n(t)\right]}{[NS3h]_{total}}\right\}=\frac{(k_b[NA]+s)}{s(n+1)(k_b[NA]+k_d+s)}\left(1+\frac{k_t}{k_d+s}\left(1-\left(\frac{k_t}{k_t+k_d+s}\right)^n\right)\right) \tag{A3}$$

In Equations (A2) and (A3), L is the Laplace transform operator and s is the Laplace variable. If rebinding of free NS3h monomers to the nucleic acid can be prevented (*e.g.*, by including a protein trap in the reaction), then we obtain a new expression for Equation (A3), shown in Equation (A4).

$$L\left\{\frac{\left[T_0^n(t)\right]}{[NS3h]_{total}}\right\}=\frac{1}{(n+1)(k_d+s)}\left(1+\frac{k_t}{k_d+s}\left(1-\left(\frac{k_t}{k_t+k_d+s}\right)^n\right)\right) \tag{A4}$$

The concentration of ADP produced by the population of NS3h monomers translocating along the nucleic acid is found by summing the amount of ADP produced by NS3h monomers at each position along the nucleic acid (Equation (A5)).

$$L\left\{\frac{[ADP(t)]}{[NS3h]_{total}}\right\}=\frac{c*k_t}{s}\sum_{i=1}^{n}T_i^n \tag{A5}$$

The substitution of Equation (A2) into Equation (A5) yields Equation (A6).

$$L\left\{\frac{[ADP(t)]}{[NS3h]_{total}}\right\}=\frac{c*k_t(k_b[NA]+s)}{s^2(1+n)(k_b[NA]+k_d+s)}\left(n-\left(\frac{k_t}{k_d+s}\right)\left(1-\left(\frac{k_t}{k_t+k_d+s}\right)^n\right)\right) \tag{A6}$$

The expression for the steady-state production of ADP by NS3h monomers translocating along the nucleic acid is linear in time and given in Equation (A7).

$$\frac{[ADP(t)]}{[NS3h]_{total}}=\left[\frac{c*k_t(k_b[NA])}{(1+n)(k_b[NA]+k_d)}\left(n-\left(\frac{k_t}{k_d}\right)\left(1-\left(\frac{k_t}{k_t+k_d}\right)^n\right)\right)\right]*t \tag{A7}$$

Equation (A6) can be rewritten as Equation (A7).

$$\frac{[ADP(t)]}{[NS3h]_{total}} = \left[(c * k_t) \left(\frac{n(1-P) - P(1-P^n)}{(1+n)(1-P)} \right) \right] \left(\frac{[NA]}{[NA] + \frac{k_d}{k_b}} \right) t \tag{A8}$$

According to Equation (A8), the production of ADP by NS3h monomers translocating along the nucleic acid has a hyperbolic dependence on the concentration of the nucleic acid. Equation (A8) can be rewritten in a simplified form as Equation (A9).

$$\frac{[ADP(t)]}{[NS3h]_{total}} = k_{cat} \left(\frac{[NA]}{[NA] + K_{0.5}} \right) t \tag{A9}$$

The parameters $K_{0.5}$ and k_{cat} in Equation (A9) are given by Equations (A10) and (A11), respectively.

$$K_{0.5} = \frac{k_d}{k_b} \tag{A10}$$

$$k_{cat} = c * k_t \left(\frac{n(1-P) - P(1-P^n)}{(1+n)(1-P)} \right) \tag{A11}$$

In the limit of infinitely long nucleic acid, (L = ∞ or equivalently, n = ∞), Equation (A11) simplifies to Equation (A12).

$$k_{cat,\infty} = c * k_t \tag{A12}$$

Equation (A10) and Equation (A12) can be combined to obtain Equation (A13).

$$\frac{k_{cat,\infty}}{K_{0.5}} = c * k_b * \frac{P}{1-P} \tag{A13}$$

Finally, Equation (A13) can be rewritten as Equation (A14) using macroscopic kinetic parameters.

$$\frac{k_{cat,\infty}}{K_{0.5}} = \left(\frac{c}{m} \right) * k_b * \frac{mP}{1-P} \tag{A14}$$

According to Equation (A14), the more processive the translocation, the larger the ratio of $\frac{k_{cat,\infty}}{K_{0.5}}$.

II. Different Probabilities for NS3h Binding to Either End of the Nucleic Acid

The first perturbation of the simple translocation model presented above is the inclusion of different probabilities for the NS3h monomer to bind to the two ends of the single-stranded nucleic acid. We define the variable *rn* as the ratio of the probability of a monomer of NS3h to bind to the 3′ end of the nucleic acid to the probability of a monomer of NS3h binding to the 5′ end of the nucleic acid. Similarly, we define the variable *r* as the ratio of the probability of a monomer of NS3h binding to any binding site on the nucleic acid, other than at the 3′ or 5′ ends, to the probability of a monomer of NS3h binding to the 5′ end of the nucleic acid. Using these definitions, we can determine expressions for the time dependence of the concentration of NS3h monomers at the various positions along the nucleic acid; these expressions are shown in Equation (A15) and Equation (A16).

$$L\left\{\frac{\left[T^{n}_{i\neq 0}(t)\right]}{[NS3h]_{total}}\right\}=\frac{(k_b[NA]+s)}{s*k_t(1+(n+1)r+rn)(k_b[NA]+k_d+s)}\left(k_t*r+((k_d+s)(rn-r)-k_t*r)\left(\frac{k_t}{k_t+k_d+s}\right)^{1-i+n}\right) \tag{A15}$$

$$L\left\{\frac{\left[T^{n}_{i=0}(t)\right]}{[NS3h]_{total}}\right\}=\frac{(k_b[NA]+s)}{s(1+(n-1)r+rn)(k_b[NA]+k_d+s)(k_d+s)}\left(k_d+k_t*r+s-\left(\frac{k_t}{k_t+k_d+s}\right)^{n}(k_t*r+(k_d+s)(r-rn))\right) \tag{A16}$$

If protein binding can be prevented, then Equation (A16) is simplified to Equation (A17).

$$L\left\{\frac{\left[T^{n}_{i=0}(t)\right]}{[NS3h]_{total}}\right\}=\frac{1}{(1+(n-1)r+rn)(k_d+s)^2}\left(k_d+k_t*r+s-\left(\frac{k_t}{k_t+k_d+s}\right)^{n}(k_t*r+(k_d+s)(r-rn))\right) \tag{A17}$$

It is worth noting that in the limit $r = rn = 1$, Equations (A15), (A16) and (A17) are identical to Equations (A2), (A3) and (A4), respectively, as expected.

As before, the concentration of ADP produced by the population of NS3h monomers translocating along the nucleic acid is found by summing the amount of ADP produced by NS3h monomers at each position along the nucleic acid. The substitution of Equation (A15) into Equation (A5) yields Equation (A18).

$$L\left\{\frac{[ADP(t)]}{[NS3h]_{total}}\right\}=\frac{c*k_t*(k_b[NA]+s)}{s^2*k_t(1+(n-1)r+rn)(k_b[NA]+k_d+s)}\left(r*k_t*n+((k_d+s)(rn-r)-k_t*r)\left(\frac{k_t}{k_d+s}\right)\left(1-\left(\frac{k_t}{k_t+k_d+s}\right)^{n}\right)\right) \tag{A18}$$

The expression for the steady-state production of ADP by NS3h monomers translocating along the nucleic acid is linear in time and displays a hyperbolic dependence on nucleic acid concentration with values of $K_{0.5}$ and k_{cat} as shown in Equation (A19) and Equation (A20), respectively.

$$K_{0.5}=\frac{k_d}{k_b} \tag{A19}$$

$$k_{cat}=\frac{c*k_t*r}{(1+(n-1)r+rn)}\left(n+((1-P)(rn-r)-r*P)\left(\frac{P}{1-P}\right)(1-P^n)\right) \tag{A20}$$

In the limit of infinitely long nucleic acid, Equation (A20) simplifies to Equation (A21).

$$k_{cat,\infty}=c*k_t \tag{A21}$$

It is worth noting that Equation (A21) is identical to Equation (A12). This result is expected since the fraction of NS3h monomers bound to either end of the nucleic acid will be zero in the limit of an infinitely long nucleic acid. Thus, under such conditions, there should be no dependence of our equation for $k_{cat,\infty}$ on the relative probabilities of binding to the ends of the nucleic acid.

III. Initiation Step Proceeding Processive Translocation

The next perturbation we consider is the inclusion of an ATP-dependent initiation process that precedes processive nucleic acid translocation by NS3h; a model for this process is shown in Scheme A2. The rate constant for the initiation process is k_i and is associated with the hydrolysis of c_i molecules of ATP. The time dependence of the concentration of NS3h at the various positions in Scheme A2 is given in Equations (A22) through (A24).

$$L\left\{\frac{\left[I_i^n(t)\right]}{[NS3h]_{total}}\right\}=\frac{(k_b[NA]+s)(k_d+s)}{s(n+1)((k_d+s)(k_2+k_i+s)+k_b[NA](k_2+k_i+s))} \tag{A22}$$

$$L\left\{\frac{\left[T_{i\neq 0}^n(t)\right]}{[NS3h]_{total}}\right\}=\frac{k_i(k_b[NA]+s)}{s(n+1)((k_d+s)(k_i+k_2+s)+k_b[NA](k_i+k_d+s))}\left(1-\left(\frac{k_t}{k_t+k_d+s}\right)^{1-i+n}\right) \tag{A23}$$

$$L\left\{\frac{\left[T_0^n(t)\right]}{[NS3h]_{total}}\right\}=\frac{k_i(k_b[NA]+s)}{s(n+1)((k_d+s)(k_i+k_2+s)+k_b[NA](k_i+k_d+s))}\left(1+\frac{k_t}{k_d+s}\left(1-\left(\frac{k_t}{k_t+k_d+s}\right)^n\right)\right) \tag{A24}$$

If we prevent rebinding by introducing a protein trap then Equation (A24) simplifies to Equation (A25).

$$L\left\{\frac{\left[T_0^n(t)\right]}{[NS3h]_{total}}\right\}=\frac{k_i}{(n+1)\,(k_d+s)\,(k_i+k_2+s)}\left(1+\frac{k_t}{k_d+s}\left(1-\left(\frac{k_t}{k_t+k_d+s}\right)^n\right)\right) \tag{A25}$$

It is worth noting that in the limit $k_i \to \infty$, Equation (A25) is identical to Equation (A4), as expected.

The concentration of ADP produced by the NS3h monomers translocating along the nucleic acid is given by Equation (A26).

$$L\left\{\frac{[ADP(t)]}{[NS3h]_{total}}\right\}=\frac{c*k_t}{s}\sum_{i=1}^{n}T_{i\neq 0}^n+\frac{c_i*k_i}{s}I_o^n \tag{A26}$$

The substitution of Equation (A22) and Equation (A23) into Equation (A26) yields Equation (A27) and Equation (A28).

$$\frac{c*k_t}{s}\sum_{i=1}^{n}T_{i\neq 0}^n=\frac{c*k_t*k_i(k_b[NA]+s)}{s^2(n+1)((k_d+s)(k_i+k_2+s)+k_b[NA](k_i+k_d+s))}\left(n-\left(\frac{k_t}{k_d+s}\right)\left(1-\left(\frac{k_t}{k_t+k_d+s}\right)^n\right)\right) \tag{A27}$$

$$\frac{c_i*k_i}{s}T_o^n=\left(\frac{c_i*k_t}{s}\right)\frac{(k_b[NA]+s)(k_d+s)}{s((k_d+s)(k_2+k_i+s)+k_b[NA](k_d+k_i+s))} \tag{A28}$$

The steady state expression for the production of ADP is linear in time and displays a hyperbolic dependence on nucleic acid concentration $K_{0.5}$ and k_{cat} as given in Equation (A29) and Equation (A30), respectively.

$$K_{0.5}=\frac{k_d(k_i+k_2)}{k_b(k_i+k_d)} \tag{A29}$$

$$k_{cat}=\left[c*k_t\left(\frac{n(1-P)-P(1-P^n)}{(1+n)(1-P)}\right)+c_i*k_d\right]\left(\frac{k_i}{k_d+k_i}\right) \tag{A30}$$

It is worth noting that in the limit $k_i \to \infty$, Equation (A29) is identical to Equation (A9), as expected. In the limit of infinitely long nucleic acid, Equation (A30) reduces to Equation (A31).

$$k_{cat,\infty}=(c*k_t+c_i*k_d)\left(\frac{k_i}{k_d+k_i}\right) \tag{A31}$$

Thus,

$$\frac{k_{cat,\infty}}{K_{0.5}} = (c * k_t + c_i * k_d)\left(\frac{k_b}{k_d}\right)\left(\frac{k_i}{k_i + k_2}\right) \tag{A32}$$

IV. Different Rate Constant for Dissociation From 5′ end

The final perturbation that we consider is when the rate constant for dissociation from the 5′ end of the nucleic acid, denoted k_{end} in Scheme A3, is different from the rate constant for dissociation from other positions along the nucleic acid. The expression for $\left[T_i^n(t)\right]$ in Scheme A3 is too cumbersome to reproduce here, but when the rebinding of dissociated NS3h to the DNA can be prevented, the expression for $\left[T_0^n(t)\right]$ is greatly simplified and is shown in Equation (A33).

$$L\left\{\frac{\left[T_0^n(t)\right]}{[NS3h]_{total}}\right\} = \frac{1}{(n+1)(k_{end}+s)}\left(1 + \frac{k_t}{k_d+s}\left(1 - \left(\frac{k_t}{k_t+k_d+s}\right)^n\right)\right) \tag{A33}$$

The steady state expression for the production of ADP is linear in time and displays a hyperbolic dependence on nucleic acid concentration. The associated values of $K_{0.5}$ and k_{cat} are dependent upon the length of the nucleic acid (*i.e.*, they are functions of n) and in the limit of infinitely long nucleic acid, are given in Equation (A34) and Equation (A35), respectively.

$$K_{0.5,\infty} = \frac{k_d}{k_b} \tag{A34}$$

$$k_{cat,\infty} = c * k_t \tag{A35}$$

Therefore,

$$\frac{k_{cat,\infty}}{K_{0.5,\infty}} = \left(\frac{c}{m}\right) * k_b * \frac{mP}{1-P} \tag{A36}$$

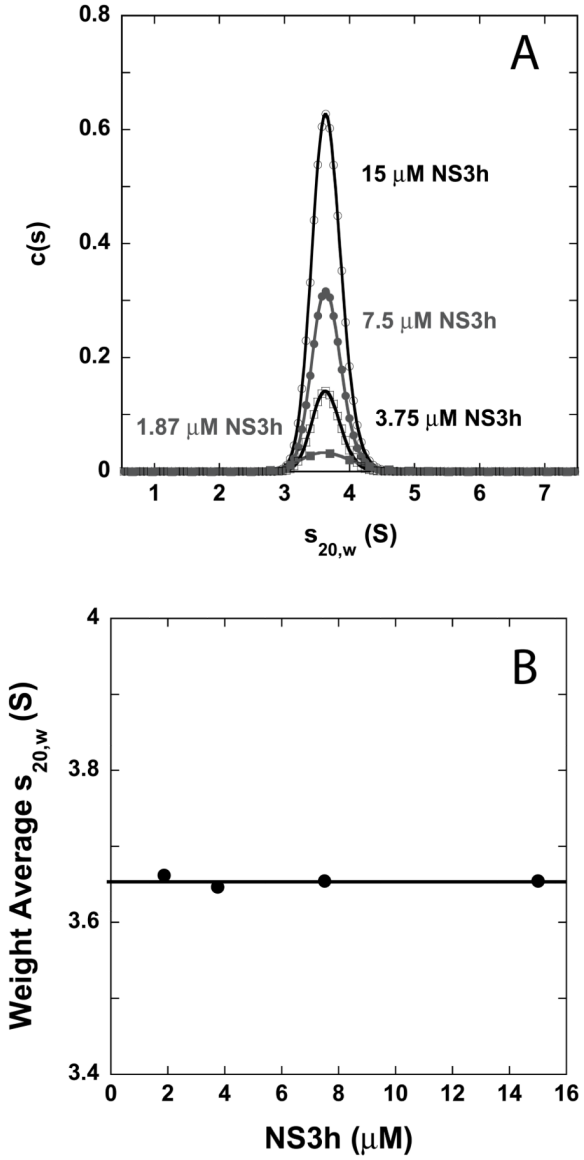

Figure 1.

NS3h is a monomer in solution. (A) The c(s) distributions resulting from the analysis of sedimentation velocity experiments conducted at 25 °C and 42,000 RPM in translocation buffer with four different total NS3h concentrations: 15 μM (black open circles), 7.5 μM (gray filled circles), 3.75 μM (black open squares), and 1.87 μM (gray filled squares). NS3h absorbance measured at 280 nm. (B) The weight average estimate of $s_{20,w}$ calculated from the further analysis of the data in (A) is independent of the total concentration of NS3h in the reaction. Taken together, these data are consistent with NS3h existing as a homogenous stable monomer in solution.

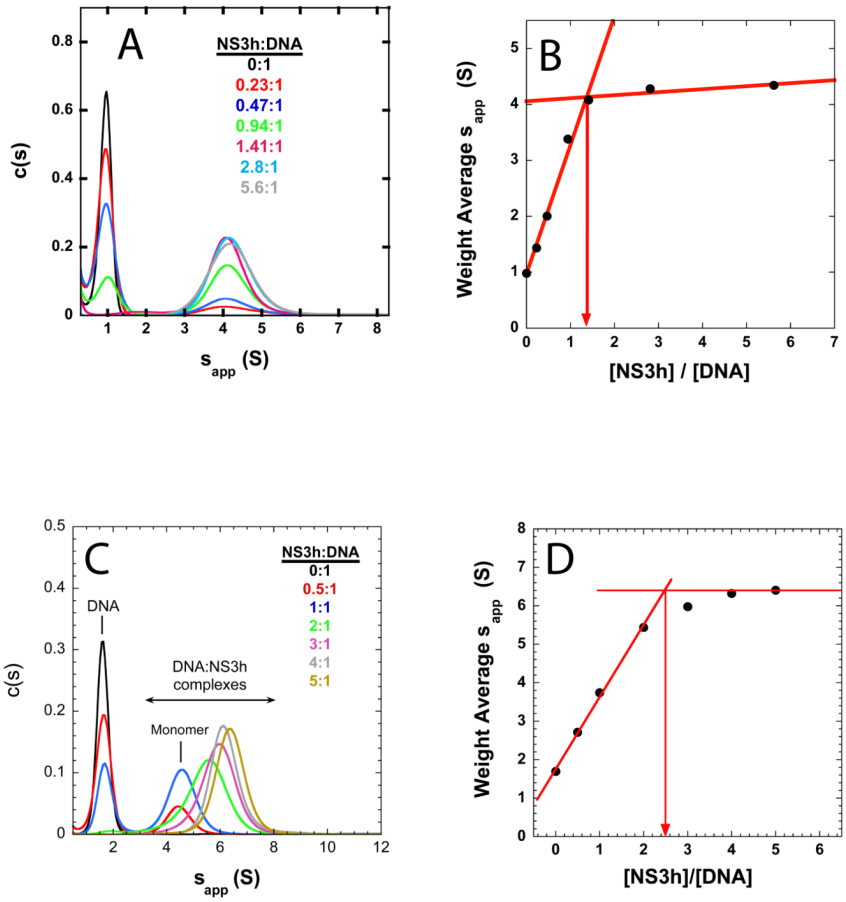

Figure 2.

Equilibrium binding of NS3h to DNA. (A) The c(s) distributions resulting from the analysis of sedimentation velocity experiments conducted at 25 °C and 48,000 RPM in translocation buffer at seven different molar concentration ratios of NS3h to 5-dT_8-Cy5: 0:1 (black), 0.23:1 (red), 0.47:1 (blue), 0.94:1 (green), 1.41:1 (pink), 2.8:1 (light blue), and 5.6:1 (gray). The concentration of 5-dT_8-Cy5 was 0.8 μM in all experiments. (B) The weight average s_{app} calculated from the further analysis of the data in (A) shows a break-point at a ratio of NS3h:DNA of 1.4:1. (C) The c(s) distributions resulting from the analysis of sedimentation velocity experiments conducted at 25 °C and 48,000 RPM in translocation buffer at seven different molar concentration ratios of NS3h to 5-ATG TGG AAA ATC TCT AGC A-Cy5: 0:1 (black), 0.5:1 (red), 1:1 (blue), 2:1 (green), 3:1 (pink), 4:1 (gray), and 5:1 (gold). The concentration of the DNA was 0.8 μM in all experiments. The absorbance of the DNA was measured at 648 nm. (D) The weight average s_{app} calculated from the further analysis of the data in (C) shows a breakpoint at a ratio of NS3h:DNA of 2.5:1.

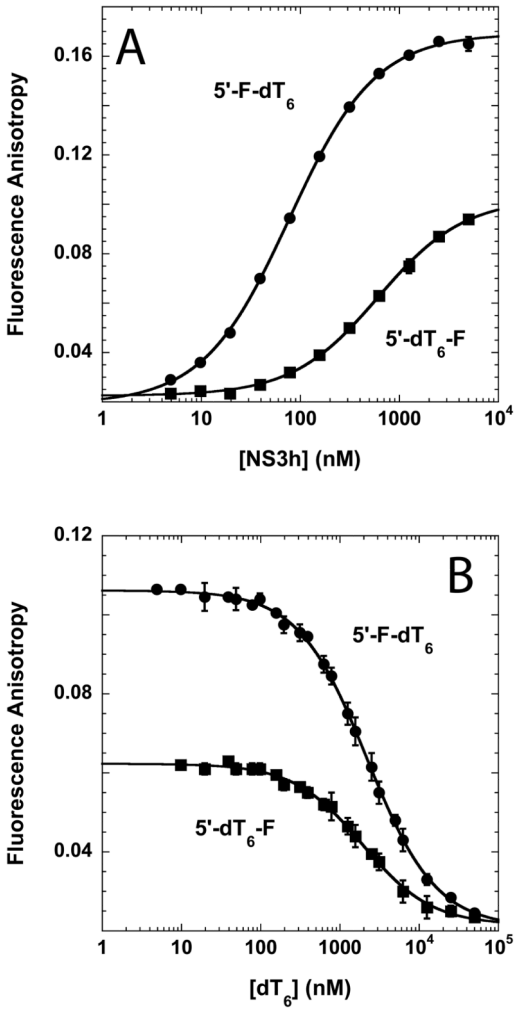

Figure 3.

Fluorescence anisotropy based measurements of the binding of NS3h to short oligonucleotides. (A) The binding of NS3h to 5′-F-dT_6 (circles) and 5′-dT_6-F (squares) as a function of the total concentration of NS3h in solution monitored by the changes in the fluorescence anisotropy of the fluorophore that occur upon the binding of NS3h to the oligonucleotides. The increase in the fluorescence anisotropy of the fluorophore is consistent with the NS3h bound oligonucleotide having a slower rotational diffusion time than the free oligonucleotide, as expected. (B) In experiments where non-fluorophore labeled oligonucleotide is included as a competitor for NS3h binding, the fluorescence anisotropy of the fluorophore labeled oligonucleotides decreases with increasing total concentration of the competitor. As shown in Table 1 and Table 2, the estimate of the affinity of NS3h binding to the unlabeled competitor molecule is independent of whether 5′-F-dT_6 or 5′-dT_6-F is used.

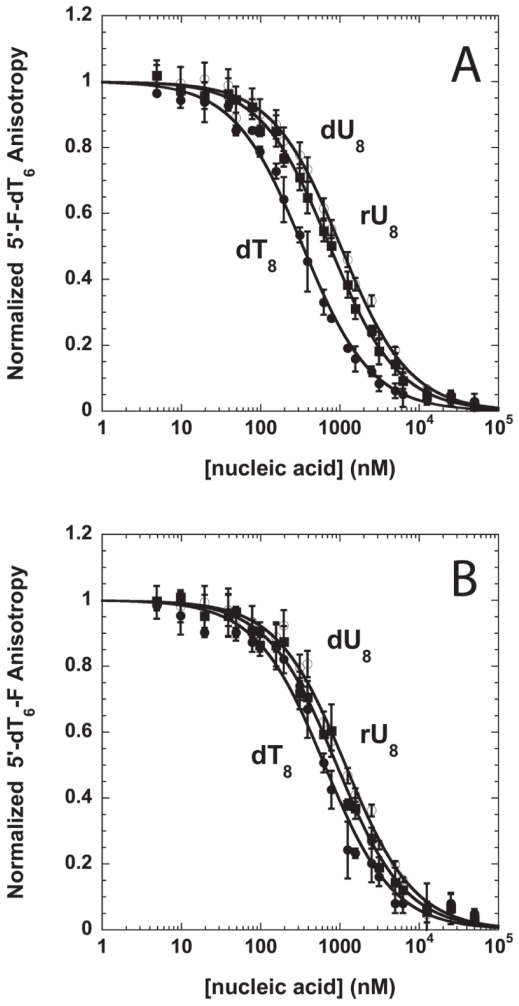

Figure 4.

Fluorescence anisotropy based measurements of the affinity of NS3h binding to dT_8 (filled circles), dU_8 (open circles) and rU_8 (squares) in competition with either 5′-F-dT_6 (A) or 5′-dT_6-F (B). Normalized fluorescence anisotropy changes are plotted as a function of unlabeled oligonucleotide concentrations. As show in Table 2, the estimates of the affinities of binding of NS3h to these short oligonucleotides are independent of whether 5′-F-dT_6 or 5′-dT_6-F are used and illustrate that the affinity of oligonucleotide binding by NS3h depends upon both the sugar and base moieties of the oligonucleotide.

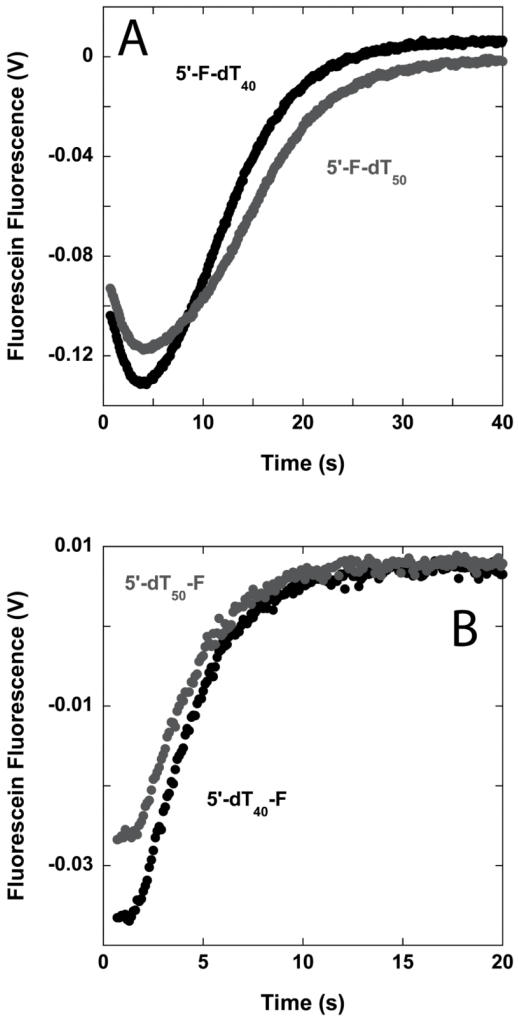

Figure 5.

The single-stranded nucleic acid translocation by NS3h is biased in the 3′ to 5′ direction. (A) Fluorescence time courses resulting from the single-round translocation of NS3h along single-stranded nucleic acids labeled on the 5′ end with fluorescein: 5′-F-dT_{40} (black) and 5′-F-dT_{50} (gray). The dependence of the time courses on the length of the nucleic acid is consistent with 3′ to 5′ directionally biased nucleic acid translocation by NS3h. (B) Fluorescence time courses resulting from the single-round translocation of NS3h along single-stranded nucleic acids labeled on the 3′ end with fluorescein: 5′-dT_{40}-F (black) and 5′-dT_{50}-F (gray). Both time courses are well described by a single-exponential increase in the fluorescence of the fluorophore with an apparent rate constant that is independent of the length of the DNA. These data are also consistent with a 3′ to 5′ directionally biased nucleic acid translocation by NS3h.

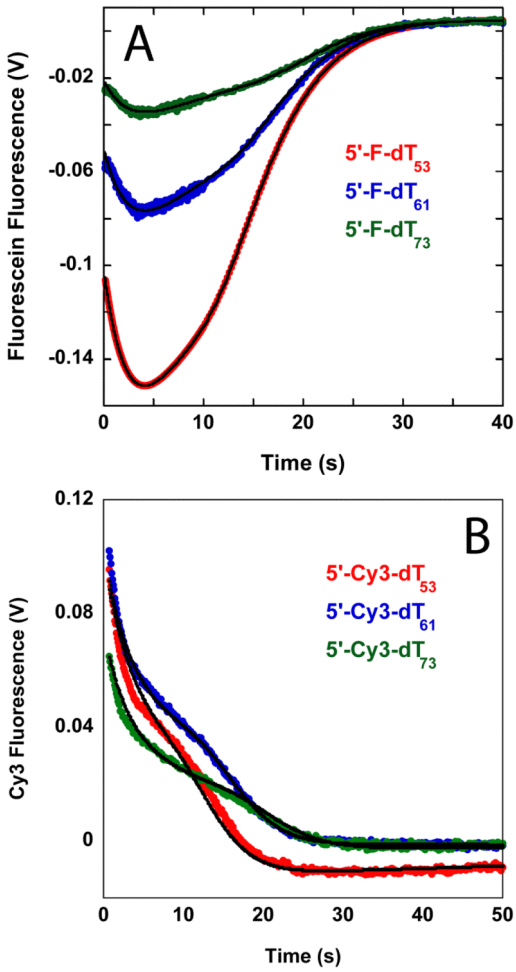

Figure 6.

NS3h translocation kinetics monitored in single-round, stopped-flow experiments with fluorophore-labeled oligodeoxythymidylates. (A) Experiments conducted with 5′-F-dT_{53} (red), 5′-F-dT_{61} (blue), and 5′-F-dT_{73} (green). (B) Experiments conducted with 5′-Cy3-dT_{53} (red), 5′-Cy3-dT_{61} (blue), and 5′-Cy3-dT_{73} (green). The solid black lines in both panels are simulations using Equation (7) and the best fit parameters obtained from the NLLS analysis of the data in the panel to Equation (7).

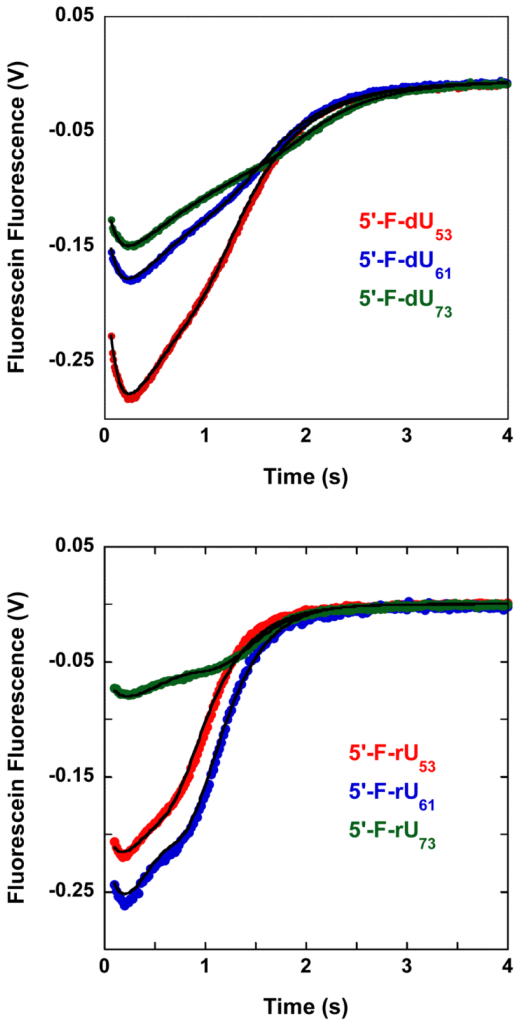

Figure 7.

NS3h translocation kinetics monitored in single-round, stopped-flow experiments with fluorophore labeled single-stranded nucleic acids. (A) Experiments conducted with 5′-F-dU_{53} (red), 5′-F-dU_{61} (blue), and 5′-F-dU_{73} (green). (B) Experiments conducted with 5′-F-rU_{53} (red), 5′-F-rU_{61} (blue), and 5′-F-rU_{73} (green). The solid black lines in both panels are simulations using Equation (7) and the best fit parameters obtained from the NLLS analysis of the data in the panel to Equation (7).

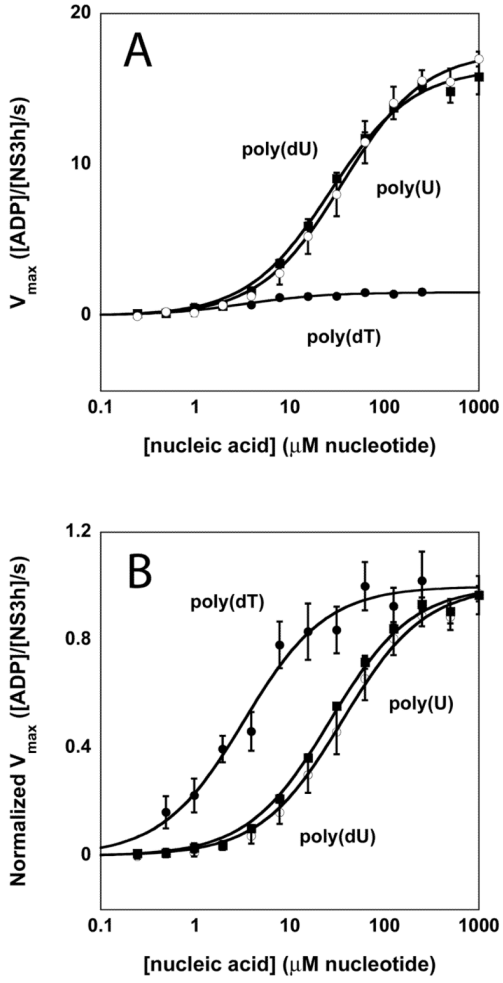

Figure 8.

The magnitude of the nucleic acid stimulated ATPase activity of NS3h depends upon the sugar and base moieties of the nucleic acid. (A) The dependence of the ATPase activity of NS3h on the total concentration of nucleic acid in the reaction. The data clearly demonstrate that the magnitude of the increase in the ATPase activity is much larger in the presence of poly(dU) (open circles) and poly(rU) (squares) than in the presence of poly(dT) (filled circles). (B) A normalized plot of the data in (A). The solid lines in both panels are simulations using Equation (11) and the best fit parameters obtained from the NLLS analysis of the data in the panel to Equation (11).

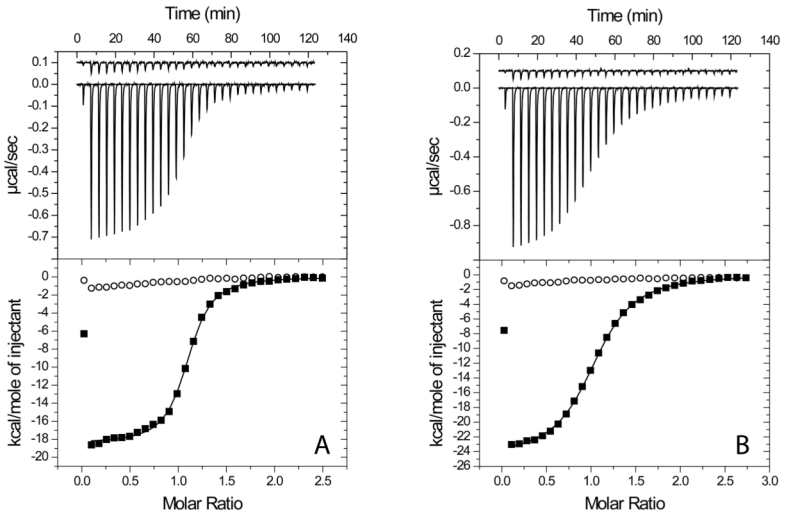

Figure 9.

Representative ITC data for $(dT)_8$ (A) and $(dU)_8$ (B) binding to NS3h. Experiments were performed in 25 mM MOPS pH 7.0, 30 mM NaCl, 5 mM $MgCl_2$, 1 mM TCEP, 1% Glycerol buffer at 25 °C. The upper panels show the raw ITC data for oligonucleotides titrated into protein, and buffer (y-axis offset). The lower panels show the integrated areas for each injection, where the solid squares represent oligonucleotide binding to protein, and the open circles represent the control experiment of oligonucleotide titrated into buffer. The solid line represents the fit to an N independent and identical binding sites model binding model, with N~1.

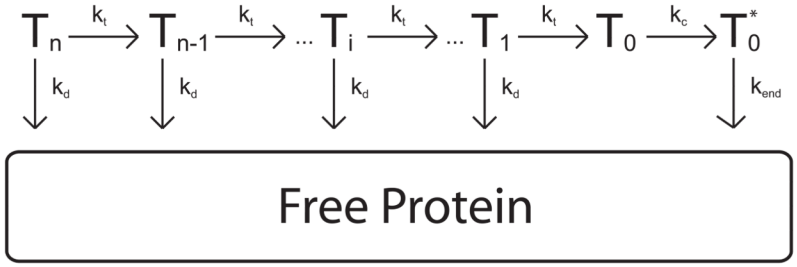

Scheme 1.

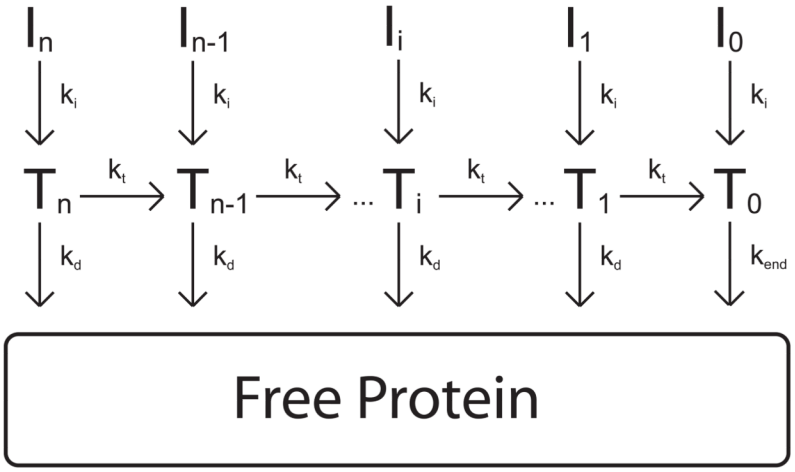

Scheme 2.

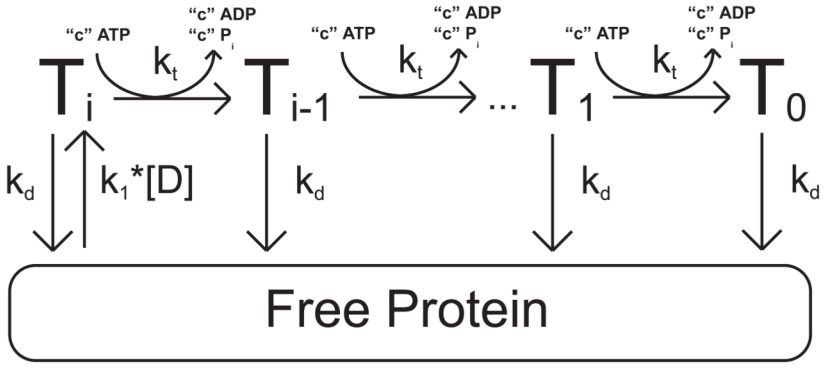

Scheme A1.

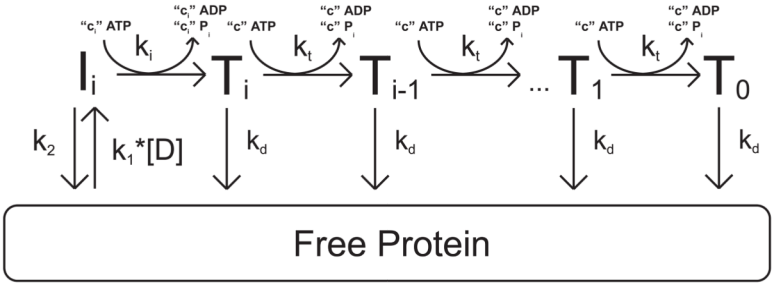

Scheme A2.

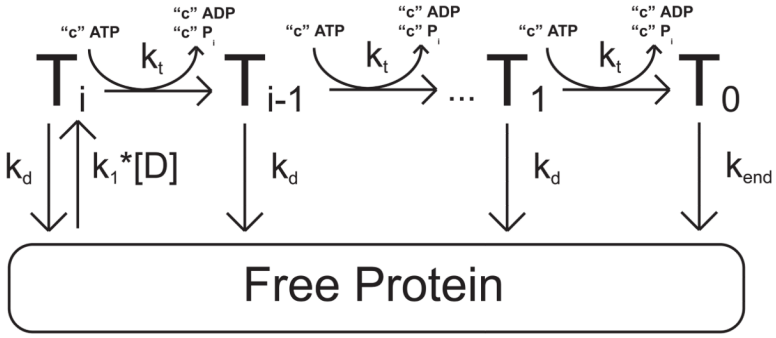

Scheme A3.

Table 1

Estimates of the affinity of NS3h binding to short oligodeoxythymidylates labeled with fluorescein at the 5′ or 3′ end or without any fluorophore label.

DNA	K_d (nM)	$K_{d,dT_6}/K_d$
5′-F-dT_6	56 ± 10	15 ± 3
3′-F-dT_6	720 ± 130	1.2 ± 0.2
dT_6	856 ± 6	1.0

The values represent the mean and associated standard deviation of the mean of the best fit parameters obtained from the analysis of two independent measurements using Equation (4) and Equation (5).

Table 2

Estimates of the affinity of NS3h binding to unlabeled short single-stranded nucleic acids determined through a competition binding assay with 5′-F-dT_6 or 5′-dT_6-F as a probe.

	K_d (nM)		
oligonucleotide	**5′-F-dT_6 competitor**	**3′-F-dT_6 competitor**	**weighted average**
dT_8	104 ± 4	167 ± 16	108 ± 4
dU_8	281 ± 13	340 ± 30	290 ± 12
rU_8	390 ± 30	480 ± 40	420 ± 20

The values represent the mean and associated standard deviation of the mean of the best fit parameters obtained from the analysis of two independent measurements using Equation (4) and (5) as described in competition binding assay section of Materials and Methods.

Table 3

Estimates of kinetic parameters associated with the translocation of NS3h along single-stranded oligonucleotides labeled on the 5′ end with either fluorescein or Cy3.

	Oligo-dT		Oligo-dU	Oligo-rU
	Fluorescein Label	**Cy3 Label**	**Fluorescein Label**	**Fluorescein Label**
k_t (steps/s)	2.4 ± 0.3	1.07 ± 0.02	36.0 ± 1.4	70 ± 4
k_d (s^{-1})	0.05 ± 0.01	0.12 ± 0.03	0.70 ± 0.03	0.31 ± 0.04
$k_{end,1} + k_2$ (s^{-1})	0.25 ± 0.04	0.402 ± 0.003	3.5 ± 1.5	2.82 ± 0.18
$k_{end,2}$ (s^{-1})	0.6 ± 0.2	0.0012 ± 0.0007	10 ± 3	14 ± 1
r	0.084 ± 0.009	0.21 ± 0.03	0.050 ± 0.008	0.030 ± 0.001
rn	0.17 ± 0.05	0.27 ± 0.14	0.14 ± 0.04	0.098 ± 0.010
m (nt/step)	1.4 ± 0.3	2.5 ± 0.1	0.96 ± 0.05	0.61 ± 0.02
d (nt)	13 ± 4	21.2 ± 1.4	14.8 ± 0.9	22 ± 3
BA	−5.6 ± 1.2	0.151 ± 0.002	−12 ± 4	−3.9 ± 0.4
m*k_t (nt/s)	3.1 ± 0.3	2.7 ± 0.2	34.2 ± 0.5	42 ± 3
P	0.980 ± 0.003	0.90 ± 0.02	0.9809 ± 0.0015	0.9956 ± 0.0008
m*P/(1−P) (nt)	80 ± 30	23 ± 4	49.4 ± 1.9	150 ± 30
1/r	12.4 ± 1.4	4.9 ± 0.7	21 ± 3	33 ± 1
rn/r	2.0 ± 0.6	2 ± 1.0	2.7 ± 0.7	3.2 ± 0.3

Values represent the mean and associated standard deviation of the mean of the best fit parameters obtained from the analysis of at least three independent data sets using Equation (7).

Table 4

Estimates of kinetic parameters associated with the translocation of NS3h along single-stranded nucleic acids labeled on the 5′ end with fluorescein.

	Oligo-dT	Oligo-dU	Oligo-rU
k_t (steps/s)	2.46 ± 0.16	35.6 ± 1.7	41 ± 2
k_d (s^{-1})	0.040 ± 0.004	0.47 ± 0.07	0.16 ± 0.03
$k_i + k_2$ (s^{-1})	0.23 ± 0.01	2.08 ± 0.08	5.6 ± 0.7
k_{end} (s^{-1})	0.31 ± 0.01	7.5 ± 1.2	3.3 ± 0.2
R	0.070 ± 0.005	0.055 ± 0.002	0.055 ± 0.009
Rn	0.18 ± 0.09	0.11 ± 0.05	0.35 ± 0.04
m (nt/step)	1.38 ± 0.07	1.00 ± 0.07	1.05 ± 0.08
d (nt)	16 ± 2	17 ± 3	29.8 ± 0.7
BA	0.402 ± 0.014	0.25 ± 0.09	0.57 ± 0.02
$m*k_t$ (nt/s)	3.35 ± 0.09	35.4 ± 0.6	42.2 ± 1.5
P	0.984 ± 0.002	0.9870 ± 0.0014	0.9961 ± 0.0005
m*P/(1−P) (nt)	90 ± 10	80 ± 20	290 ± 50
1/r	14 ± 1	18.3 ± 0.7	19 ± 2
rn/r	3 ± 1	2.0 ± 0.8	7 ± 1

Values represent the mean and associated standard deviation of the mean of the best fit parameters obtained from the analysis of at least three independent data sets using Equation (9).

Table 5

Estimates of the steady-state kinetic parameters associated with the polynucleic acid stimulated ATPase activity of NS3h.

Nucleic Acid	$k_{cat,\infty}$ ([ADP]/[NS3h]/s)	$K_{0.5}$ (μM nucleotide)	$\frac{k_{cat,\infty}}{K_{0.5}}$ (10^4 [ADP] [NS3h]$^{-1}$ [NA]$^{-1}$ s^{-1})
Poly(dT)	1.54 ± 0.04	3.3 ± 0.4	46 ± 5
Poly(dU)	16.4 ± 0.2	30.0 ± 1.0	55 ± 2
Poly(rU)	17.5 ± 0.2	36.0 ± 2.0	49 ± 3

The values represent the average and standard deviation of the best fit parameters obtained from the analysis of at least 4 independent measurements using Equation (11). [NA] is the concentration of the nucleic acid.

Table 6

Estimates of the macroscopic efficiency of ATP coupling to single-stranded nucleic acid translocation by NS3h. The estimates are obtained through a combined analysis of the data in Table 3, Table 4, and Table 5.

	Scheme 1		Scheme 2	
Nucleic Acid	***m* k*$_t$ (nt/s)**	$\left(\frac{k_{cat,\infty}}{m*k_t}\right)=\left(\frac{c}{m}\right)$ **[ADP]/[NS3h]/nt**	***m* k*$_t$ (nt/s)**	$\left(\frac{k_{cat,\infty}}{m*k_t}\right)\left(\frac{k_i+k_d}{k_i}\right)=\left(\frac{c}{m}\right)$ **[ADP]/[NS3h]/nt**
oligo(dT)	3.1 ± 0.3	0.50 ± 0.05	3.35 ± 0.09	0.53 ± 0.03
oligo(dU)	34.2 ± 0.5	0.478 ± 0.009	35.4 ± 0.6	0.57 ± 0.03
oligo(rU)	42 ± 3	0.42 ± 0.03	42.2 ± 1.5	0.427 ± 0.015

Table 7

Estimates of the equilibrium thermodynamic parameters associated with the binding of NS3h to short single stranded nucleic acids as determined from isothermal titration calorimetry.

Substrate	N	K_{eq} (10^6 M^{-1})	ΔG^0 (kcal/mol)	ΔH^0 (kcal/mol)	$T\Delta S^0$ (kcal/mol)
dT_8	1.07 ± 0.01	7.2 ± 0.3	−9.34 ± 0.02	−18.4 ± 0.2	−9.1 ± 0.2
dU_8	1.01 ± 0.04	1.9 ± 0.2	−8.55 ± 0.06	−25.5 ± 1.2	−17.0 ± 1.2
rU_8	0.93 ± 0.01	1.37 ± 0.08	−8.36 ± 0.03	−25 ± 2	−17 ± 2